AD-A114 640 CHARLES STARK DRAPER LAB INC CAMBRIDGE MA F/G 17/2
EVALUATION OF AN ADVANCED GYRO AND WHEEL SPEED MODULATION FOR H--ETC(U)
DEC 81 J SHEARER F19628-81-K-0008
UNCLASSIFIED CSDL-R-1530 AFGL-TR-82-0016 NL

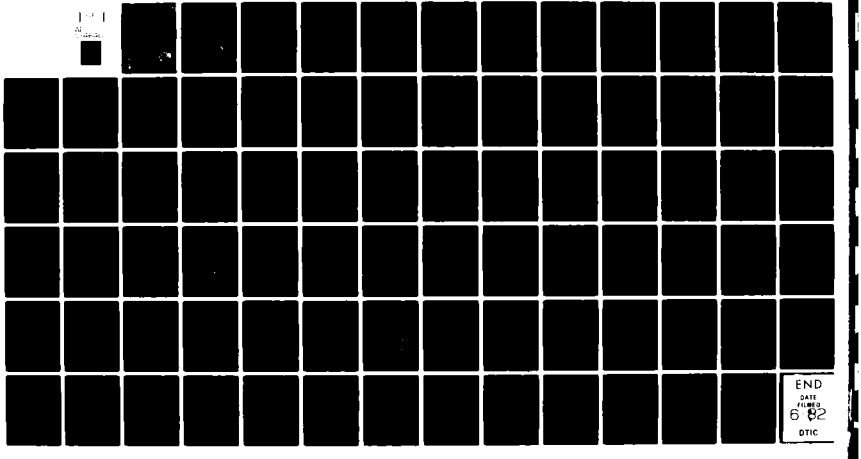

END
DATE FILMED
6 82
DTIC

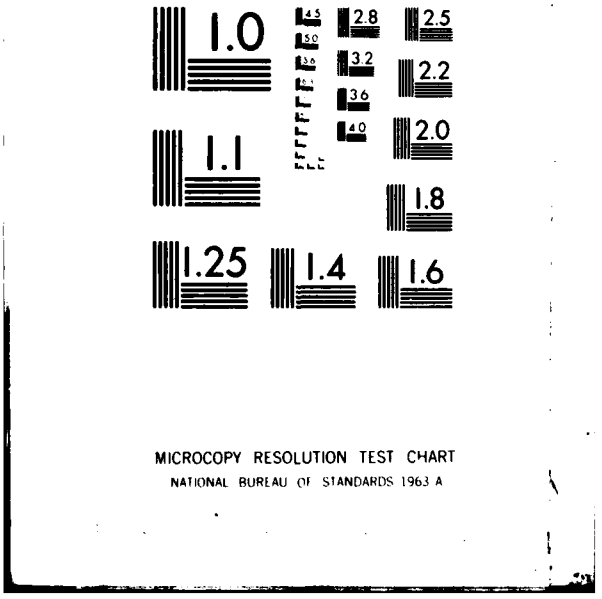
1.0
1.1
1.25
1.4
1.6
1.8
2.0
2.2
2.5
2.8
3.2
3.6
4.0
4.5
5.0
MICROCOPY RESOLUTION TEST CHART
NATIONAL BUREAU OF STANDARDS 1963 A

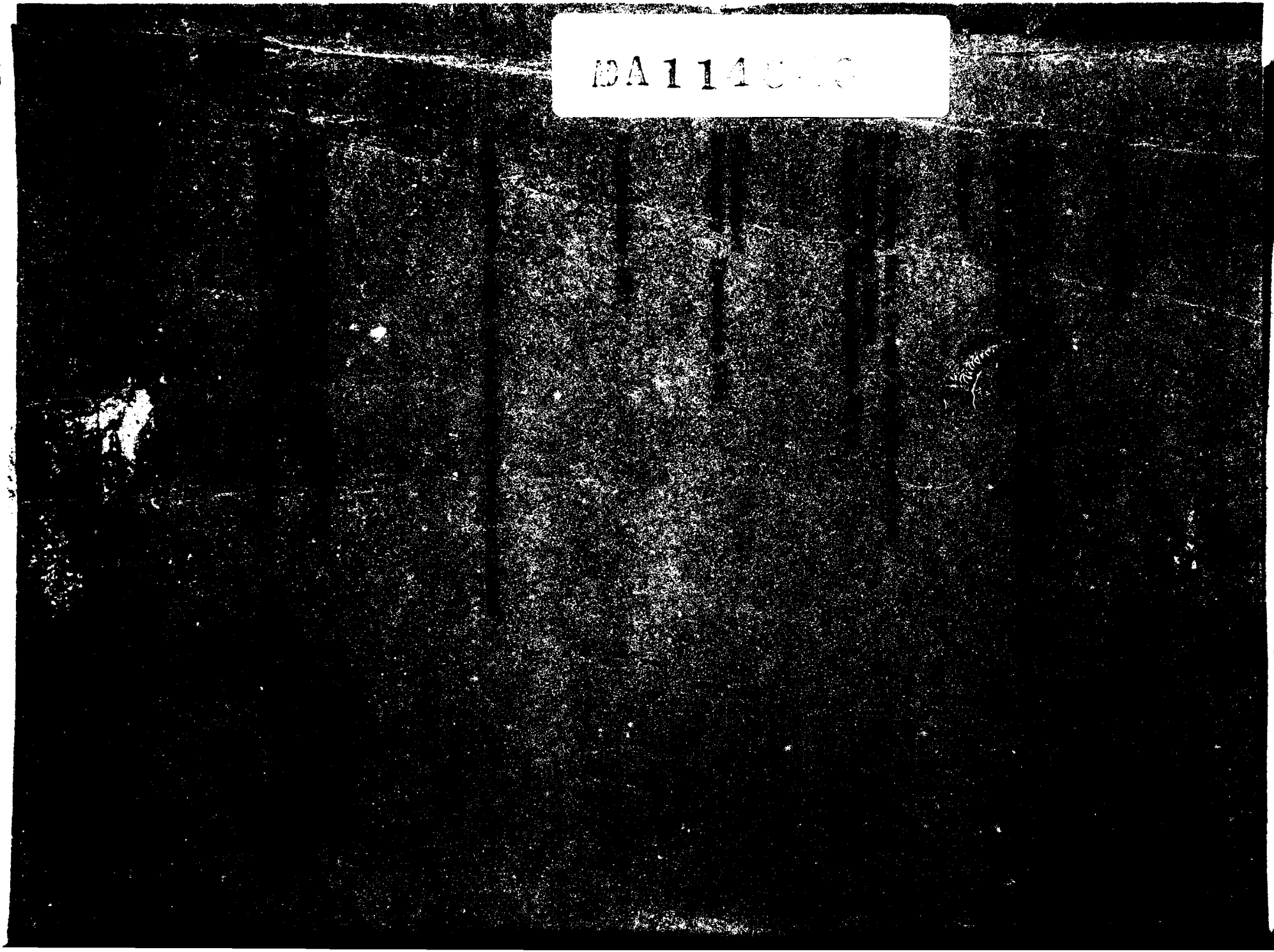
AD A114

UNCLASSIFIED

SECURITY CLASSIFICATION OF THIS PAGE *(When Data Entered)*

REPORT DOCUMENTATION PAGE

READ INSTRUCTIONS BEFORE COMPLETING FORM

1. REPORT NUMBER: AFGL-TR-82-0016	2. GOVT ACCESSION NO.: AD-A114640
3. RECIPIENT'S CATALOG NUMBER:	
4. TITLE *(and Subtitle)*: Evaluation of an Advanced Gyro and Wheel Speed Modulation for Highly Accurate Azimuth Determination	5. TYPE OF REPORT & PERIOD COVERED: Final Report 26 Jan - 31 Dec 1981
	6. PERFORMING ORG. REPORT NUMBER: CSDL-R-1530
7. AUTHOR(s): J. Shearer	8. CONTRACT OR GRANT NUMBER(s): F19628-81-K-0008
9. PERFORMING ORGANIZATION NAME AND ADDRESS: The Charles Stark Draper Laboratory, Inc. 555 Technology Square Cambridge, MA 02139	10. PROGRAM ELEMENT, PROJECT, TASK AREA & WORK UNIT NUMBERS: 62101F 760010AB
11. CONTROLLING OFFICE NAME AND ADDRESS: Air Force Geophysics Laboratory Hanscom, Ma 01731 Monitor: Capt. J. Novak/LWH	12. REPORT DATE: 31 December 1981
	13. NUMBER OF PAGES: 80
14. MONITORING AGENCY NAME & ADDRESS *(if different from Controlling Office)*: ONRRR Massachusetts Institute of Technology Room E19-628 Cambridge, MA 02139	15. SECURITY CLASS. *(of this report)*: Unclassified
	15a. DECLASSIFICATION/DOWNGRADING SCHEDULE

16. DISTRIBUTION STATEMENT *(of this Report)*

APPROVED FOR PUBLIC RELEASE: DISTRIBUTION UNLIMITED

17. DISTRIBUTION STATEMENT *(of the abstract entered in Block 20, if different from Report)*

18. SUPPLEMENTARY NOTES

19. KEY WORDS *(Continue on reverse side if necessary and identify by block number)*

Azimuth Measurement
Wheel Speed Modulation
Permanent Magnet Wheel Gyroscope
Geophysics
Earth Motion Measurement

20. ABSTRACT *(Continue on reverse side if necessary and identify by block number)*

This report presents the results of a feasibility study which evaluated the technique of Wheel-Speed Modulation (WSM) of a CSDL-designed Permanent Magnet (PM) wheel gyroscope for measurement of true astronomic azimuth to state-of-the-art accuracy. The report describes a detailed performance model for WSM operation of the gyro, and a series of unique tests which were especially designed to evaluate (1) the repeatability of the gyro torque across repeated speed changes, (2) the long-term stability of the known error parameters (over)

DD FORM 1 JAN 73 1473 EDITION OF 1 NOV 65 IS OBSOLETE

UNCLASSIFIED

SECURITY CLASSIFICATION OF THIS PAGE *(When Data Entered)*

associated with WSM, and (3) the accuracy of the WSM technique as compared with traditional four-position gyrocompassing.

The test data demonstrated that true azimuth can be measured to a precision of at least 0.75 arc seconds (one sigma) in an hour or less for a period of at least four consecutive days during quiescent conditions. The data also confirmed that the torque bias shift which arises from changing the gyro wheel speed is very repeatable. Thus, once this bias is calibrated, the gyro can be operated automatically using WSM to accurately track the azimuthal motions of the test article without interruption for extended periods.

Some anomalous gyro torque data were observed whenever environmental changes (tilt and temperature) occurred. No conclusions can be reached at this time as to whether this anomalous behavior was the result of an inadequately or incorrect performance model, or the inability to accurately measure and compensate for tilt and tilt rate errors.

However, the demonstrated performance confirms that WSM is a feasible alternative for the advancement of azimuth measurement technology, and that existing hardware and techniques can be integrated into an azimuth measuring system which can meet the requirements of the 1980's.

SUMMARY OF RESULTS

The investigation consisted of a series of tests which were designed to evaluate the capability of measuring true azimuth to state-of-the-art accuracy using the technique of Wheel-Speed-Modulation (WSM) developed by CSDL with a CSDL Permanent Magnet (PM) wheel gyroscope. The test data demonstrated that true azimuth can be measured to a precision of at least 0.75 arc seconds (one sigma) in an hour or less for a period of at least four consecutive days during quiescent conditions.

The investigation consisted of developing a detailed performance model for WSM operation of the gyro, and a series of tests to evaluate (1) the repeatability of the gyro torque across repeated speed changes, (2) the long-term stability of the known error parameters associated with WSM, and (3) the accuracy of the WSM technique as compared with traditional four-position gyrocompassing.

The performance model for WSM was developed and is presented herein. There is some doubt, however, whether this model is complete since anomalous gyro torque data were observed whenever environmental changes (tilt and temperature) occurred. No conclusions can be reached at this time as to whether this anomalous behavior was the result of an inadequate or incorrect performance model, or the inability to measure and compensate for tilt and tilt rate errors.

The test data overwhelmingly confirmed that the $\Delta_K D_F$ error term which arises from changing the gyro wheel speed is very repeatable across multiple speed changes, and is stable for periods exceeding several weeks as long as the gyro is continuously run. The upper limit of this stability is not known since this was not specifically evaluated. This long-term stability means that $\Delta_K D_F$ need be calibrated only once at the beginning of a test series or azimuth measurement program. The gyro can then be operated automatically using WSM to accurately track the azimuthal motions of the test article or reference without interruption for extended periods.

The stability across power shutdowns was examined only once due to startup abnormalities which occurred with this particular test gyro. No noticeable change in $\Delta_K D_F$ occurred across this shutdown.

The data suggests that the azimuth uncertainty is smaller for full-to-quarter WSM than full-to-half WSM. This is a desirable condition since the resolution of small earth rate inputs is greater with increased separation of the wheel speeds.

Although integration periods shorter than one hour were not attempted in this investigation, it appears that the measurement time at each wheel speed can be reduced significantly without degrading accuracy. Since the gyro transients associated with the speed changes have time constants of less than 10 minutes, it is reasonable to assume that an accurate azimuth estimate can be obtained every 15 minutes with this test gyro. Float suspension system modifications already incorporated in other CSDL PM gyros could allow reduction of this measurement time even further.

The above results confirm that WSM is a feasible alternative for the advancement of azimuth measurement technology, and that existing hardware and techniques can be integrated into an azimuth measuring system which can meet the requirements of the 1980's.

TABLE OF CONTENTS

List of Figures

List of Figures (Cont.)

EVALUATION OF AN ADVANCED GYRO AND WHEEL SPEED MODULATION FOR HIGHLY ACCURATE AZIMUTH DETERMINATION

1. INTRODUCTION

The Component Development Department, Test and Analysis Division of the Charles Stark Draper Laboratory, Inc. (CSDL), conducted an engineering evaluation of an advanced gyroscope and technique for accurately determining astronomic azimuth. The evaluation was conducted on a specially configured test station located at CSDL, during the period January through September 1981, under Contract F19628-81-K-0008 with the Air Force Geophysics Laboratory (AFGL), Hansom AFB, Massachusetts.

1.1 Objective

The objective of the investigation was to evaluate the feasibility of using an advanced CSDL gyroscope with a Permanent Magnet (PM) wheel in combination with the technique of Wheel-Speed Modulation (WSM) for precise measurement of astronomic azimuth. Specifically, the study assessed the improvement in accuracy and the reduction in measurement time which could be achieved by using a PM gyro and WSM in an advanced inertial azimuth measuring system. The a priori goal was to demonstrate a measurement uncertainty of one arc second or less in approximately one hour in the test laboratory.

The evaluation consisted of four major thrusts: (a) to design, fabricate and test breadboard electronics to operate the permanent magnet wheel gyroscope and to automatically modulate the wheel speed from full speed to two-thirds, one-half or one-fourth speeds; (b) to develop a model of expected behavior for the gyro in the designated test configuration and to assess the validity of this model using actual test data; (c) to conduct a series of engineering tests with the permanent magnet gyro in order to assess its capability for measuring small azimuth changes with WSM; and (d) to assess the optimum azimuth measurement capability and feasibility of incoporating the CSDL prototype or similar PM into an advance version of the AFGL Automated Azimuth Measuring System (AAMS). Each of these tasks is discussed in detail in the following sections.

1.2 Principle of WSM

Wheel Speed Modulation is a mode of operating the gyroscope whereby the rate about the input axis (in this case earth rate) can be precisely determined by iteratively changing the angular momentum of the gyro wheel and by measuring the resulting change in gyro torque. The wheel angular momentum is directly proportional to the wheel angular rate, and thus it can be easily changed by changing the speed of the wheel. However, some complications occur with conventional gyros which do not occur with the PM gyro.

Conventional gyros contain a hysteresis-ring, synchronous motor which maintains the gyro wheel at high angular velocities. The angular velocity or speed can be varied through the excitation frequency, but the uncertainty of gyro drift is adversely affected by changing the wheel speed. This occurs because each time the wheel hysteresis ring and rotor synchronize with the rotating stator magnetic field, a residual magnetic field is formed. Since the rotor is magnetically soft, the residual magnetic field is reformed with a different strength and angle with respect to the stator field with each synchronization. An input current change results, and a torque is produced by the change in flex-lead current and motor-power dissipation. This torque is related to rate uncertainty through the wheel angular momentum. Thus, even accurate and repeatable frequency changes result in power or current changes which are unpredictable, and accurate azimuth measurement using WSM with a conventional gyro is impossible.

In contrast, the Permanent Magnet (PM) gyro wheel is magnetically hard, thereby greatly reducing the magnetic field variations with repeat rotor-stator synchronization. A closed-loop method of motor control is used where the amplitude of the stator field is controlled by a speed-control loop. With the rotor at synchronous speed, back EMF is used to sense the PM-motor angular position which is then compared to the phase of a clock to produce a speed-control signal. Frequency and angle of the stator current are matched to the rotor position, making the change in gyro torque due to the wheel speed change inherently much more repeatable than with the conventional gyro.

Using a PM wheel motor further improves gyro performance because of its efficiency and repeatability between turn-ons. The prototype PM wheel motor tested at CSDL showed better than 0.1 milliwatt power repeatability at an operating level of roughly 2 watts. Because the operating power is low and efficiency is high, variations in wheel speed cause comparatively small power variations. These features reduce torque uncertainties during wheel-speed modulation by decreasing transient effects, which enhances measurement accuracy.

The majority of the test data acquired for this evaluation used WSM between either full and one-half speeds or full and one-quarter speeds. A complete description of the gyro rebalance equations for each combination of WSM are presented in Section 3 of this report.

2. INSTRUMENTATION

The first major sub-task involved reconfiguration of the gyro test station. This involved developing a new set of electronics to automatically operate the gyro and change the wheel speed. In addition, since accuracy to less than one arc second was desired, a means of precise table alignment was needed. This was achieved by adding the capability of automatically repositioning the test table to predetermined orientations repeatedly during the test. Finally, an expanded digital data acquisition system was integrated with the test station. This LSI-11 based system controlled all data acquisition, converted analog signals to digital data, pre-filtered the data and stored all data on magnetic tape for later post-processing. The computer data acquisition system also enabled automated, remote control of the test sequence, thereby minimizing the corruptive influences of personnel activity at the test station.

In its final configuration, the test station consisted of modified gyro test table, gyro support electronics, four AFGL-furnished Radian C-3 tiltmeters, an autocollimator, a train detector, and the LSI-11 microprocessor. Twenty-one channels of data were collected, including gyro torque, gyro float position parameters, gyro and ambient temperatures, gyro wheel power, gyro heater power, table tilt, table position as monitored by an autocollimator, and a railroad train detector signal.

Data acquisition rates and output rates were varied throughout the test, but the majority of the data were sampled at 1 second intervals, pre-filtered to 10 seconds, and post-filtered to 100 second and/or 1 hour intervals. The only exception was the digital gyro torque, which was determined by accumulating pulses over a given integration period from the continuous 400 Hz pulse train emitted from the gyro torquer.

A modified version of a CSDL single-degree-of-freedom gyro was selected as the test gyroscope. This gyro, designated as PM-1, was built as a pre-prototype to the fourth generation gyro family. The major significant configuration change was the replacement of the hysteresis wheel with a permanent magnet wheel. This modification ensured repeatable torque signals at each wheel speed.

3. GYRO TORQUE AND AZIMUTH MODEL EQUATIONS FOR WSM

This section develops the gyro performance model equation while in a fixed orientation, but with periodic, iterative changes in the gyro wheel speed. The equations derived below apply to operation of the gyro with the Input Axis (IA) either east or west, the Spin Axis (SA) either north or south and the Output Axis (OA) either up or down. Thus, IA and SA are approximately in the local level plane (as determined by the tiltmeters), and OA is approximately in the local vertical plane. These test orientations are standard orientations used for traditional four-position gyrocompassing.

3.1 Simplified Rebalance Torque Equation for WSM

The rebalance torque for a gyro operating in torque-to-balance mode is

$$M(\text{dyne-cm}) = H\left(\frac{\text{dyne-cm}}{\text{meru}}\right)\omega_{IA}\,(\text{meru}) + D_F\,(\text{dyne-cm}) \qquad (1)$$

$$+ \Sigma D_{UNB}\left(\frac{\text{dyne-cm}}{\text{cm/sec}^2}\right) a_i\left(\frac{\text{cm}}{\text{sec}^2}\right) + \Sigma D_{COMP}\left(\frac{\text{dyne-cm}}{\text{cm}^2/\text{sec}^4}\right) a^2{}_i\left(\frac{\text{cm}^2}{\text{sec}^4}\right) + \ldots$$

where

M = rebalance torque

H = angular momentum of the wheel = 0.026 $\frac{\text{dyne-cm}}{\text{meru}}$ for PM-1

ω_{IA} = input axis angular rate

D_F = gyro drift

D_{UNB} = drift due to mass unbalance along each of the three gyro axes per unit acceleration

D_{COMP} = drift due to compliance along each of the three gyro axes per unit acceleration squared

If the gyro wheel speed is then reduced to some new speed by a specified constant K, then the angular momentum is also reduced such that $H_2 = KH_1$, and the new torque can be expressed by

$$M_2 = KH\omega_{IA} + D_F + \Delta_K D_F + \Sigma D_{UNB}\, a_i + \Sigma \Delta_K D_{UNB}\, a_i + \Sigma D_{COMP}\, a_i^2 + \Sigma \Delta_K D_{COMP}\, a_i^2 \qquad (2)$$

where the Δ_K terms are the change in drift due to the new wheel speed defined by K.

The simplified model equation for WSM can then be represented as Equation (1) - Equation (2), or

$$\Delta M = (1-K)H\omega_{IA} - \Delta_K D_F \qquad (3)$$

where the acceleration dependent terms are neglected since their difference across wheel speed changes are trivial.

D_F, on the other hand, varies significantly with wheel speed, and thus $\Delta_K D_F$ cannot be neglected. This term arises due to changes in heater power, wheel power and flex lead current across wheel speed modulations. Repeatability of this term at each desired wheel speed is, in fact, critical to the ability to measure azimuth to the desired level of accuracy. Thus, $\Delta_K D_F$ repeatability was a key test parameter.

3.2 Gyro Input Axis Rates

With the gyro in the local level plane and the input axis pointed east, the cumulative rate about the gyro input axis at any point in time is

$$\omega_{IA} = \sin \alpha \, \omega_{erh} + \sin \beta \, \omega_{erv} + \omega_{\gamma} \tag{4}$$

where

α = azimuth deviation from east

β = tilt angle about the spin axis (north-south)

γ = tilt about the input axis (east-west)

ω_{erh} = horizontal component of earth rate = $\omega_e \cos L$

ω_{erv} = vertical component of earth rate = $\omega_e \sin L$

L = latitude angle

ω_{γ} = tilt rate about the input axis

From Equation (4) it is apparent that the rate about IA due to tilt and tilt rate cannot be separated from the azimuth component of earth rate, and thus the torques due to tilts and tilt rates are also indistinguishable from the azimuth torque which we are trying to observe.

3.3 WSM Torque Equations

To evaluate the effects of these motions on the WSM torque, let us consider the special case where the speed is modulated between full and half speed. From Equations (1) and (2), the general torque equations, including the effects of tilt, and neglecting gyro error torques (which later drop out) are

$$M_F = H\omega_{IA} + D_F = H[\omega_e \cos L \sin \alpha + \omega_e \sin L \sin \beta_F + \omega_{\gamma_F}] + D_F \tag{5}$$

$$M_H = \frac{H}{2}\omega_{IA} + D_F + \Delta D_F = \frac{H}{2}(\omega_e \cos L \sin \alpha + \omega_e \sin L \sin \beta_H + \omega_{\gamma_H}) + D_F + \Delta_H D_F \tag{6}$$

$$\Delta M_{F/H} = H[\tfrac{1}{2}\,\omega_e \cos L \sin\alpha + \omega_e \sin L\,(\sin\beta_F - \tfrac{1}{2}\sin\beta_H)$$

$$+ \omega_{\gamma_F} - \tfrac{1}{2}\,\omega_{\gamma_H}] - \Delta_H D_F \qquad (7)$$

where

$M_{F,H}$ = torque at full or half wheel speed, respectively

$\beta_{F,H}$ = tilt at full or half wheel speed, respectively

$\omega_{\gamma_{F,H}}$ = tilt rate at full or half wheel speed, respectively

From equation (7), it is apparent that the motions of concern for WSM are actually the differences between the tilts (or rates) at full vs half wheel speed rather than the absolute values, and that the effects of both tilt and rate are twice as large at full wheel speed as at half speed. Further, the tilt correction is approximately equal to $2\beta_F - \beta_H$ which is not an observable quantity. Our observable is $(\beta_F - \beta_H)$, and the error in absolute azimuth is then approximately equal to the tilt effect of β_F, which would look like a bias in our azimuth estimate.

The equations for WSM between full and quarter wheel speeds can be similarly derived as follows, where subscripts F and Q represent full and quarter speeds respectively.

$$M_F = H[\omega_e \cos L \sin\alpha + \omega_e \sin L \sin\beta_F + \omega_{\gamma_F}] + D_F \qquad (8)$$

$$M_Q = \tfrac{H}{4}[\omega_e \cos L \sin\alpha + \omega_e \sin L \sin\beta_Q + \omega_{\gamma_Q}] + D_F + \Delta_Q D_F \qquad (9)$$

$$\Delta M_{F/Q} = H[\tfrac{3}{4}\omega_e \cos L \sin\alpha + \omega_e \sin L\,(\sin\beta_F - \tfrac{1}{4}\sin\beta_Q)$$

$$+ \omega_{\gamma_F} - \tfrac{1}{4}\omega_{\gamma_Q}] - \Delta_Q D_F \qquad (10)$$

In general, one can conclude from Equations (7) and (10) that the greater the separation between the full and reduced speeds, the more the WSM delta torque error is dependent upon the tilt and rate at full wheel speed. This points to the need for accurate tilt and tilt rate measurements as part of an azimuth measuring system.

3.4 WSM Azimuth Equations

The azimuth deviation of the gyro input axis from true east can now be derived for the two special cases used in this evaluation by solving Equations (7) and (10) for sin α. FOR WSM between full and half speeds, the azimuth is

$$\alpha \approx \sin\alpha = \frac{2(\Delta M_{F/H} + \Delta_H D_F)}{H\omega_e \cos L} - \tan L\,(2\sin\beta_F - \sin\beta_H)$$

$$- \frac{2\omega_{\gamma_F} - \omega_{\gamma_H}}{\omega_e \cos L} \qquad (11)$$

For WSM between full and quarter speeds, the azimuth is

$$\alpha \approx \sin\alpha = \frac{4}{3}\,\frac{\Delta M_{F/Q} + \Delta_Q D_F}{H\omega_e \cos L} - \frac{\tan L}{3}\,(4\sin\beta_F - \sin\beta_Q)$$

$$- \frac{4\omega_{\gamma_F} - \omega_{\gamma_Q}}{3\omega_e \cos L} \qquad (12)$$

In general, the azimuth equation for WSM is then

$$\alpha \approx \sin\alpha = \left(\frac{1}{1-K}\right)\frac{\Delta M_{F/K} + \Delta_K D_F}{H\omega_e \cos L} - \tan L\left(\frac{\sin\beta_F}{1-K} - \frac{K\sin\beta_K}{1-K}\right.$$

$$- \frac{\omega_{\gamma_F}}{(1-K)\omega_e \cos L} + \frac{K\omega_{\gamma_K}}{(1-K)\omega_e \cos L} \qquad (13)$$

where typical wheel speed constants are

K	$\frac{1}{1-K}$
3/4	4
2/3	3
1/2	2
1/4	4/3

4. ENGINEERING TEST PROGRAM

The engineering test program began in July 1981 and continued through September 30, 1981. This segment of the evaluation was intended for verification of the WSM model equations and assessment of the azimuth measuring accuracy of the PM gyro. The test program consisted of the following segments, each of which is described in some detail in the ensuing sections of this report: (1) Characterization of Test Station Tilt Environment, (2) Preliminary Gyro Evaluation and Preparation for WSM Tests, (3) Steady State (Fixed Position) WSM Tests, (4) Gyrocompassing with WSM, (5) Angle Measurement with WSM, (6) $\Delta_K D_F$ Repeatability Across Power Shutdown, (7) Assessment of Selected Reduced Wheel Speeds, (8) Transient Analysis, and (9) Evaluation of Environmental Effects on Azimuth Measurement by WSM.

4.1 Characterization of Test Station Tilt Environment

Tilt characterization was accomplished by a preliminary measurement evaluation prior to gyro testing and by continuous measurements throughout the gyro test program.

Two of the GFE tiltmeters were operated intermittently during the preliminary characterization during periods when the station was not disturbed. Tilts were typically smaller than 2 arc seconds peak-to-peak with dominant period of 24 hours. Figures 1 and 2 are plots of typical tilts observed on the test table. These data were taken over a weekend starting 17 July 1981.

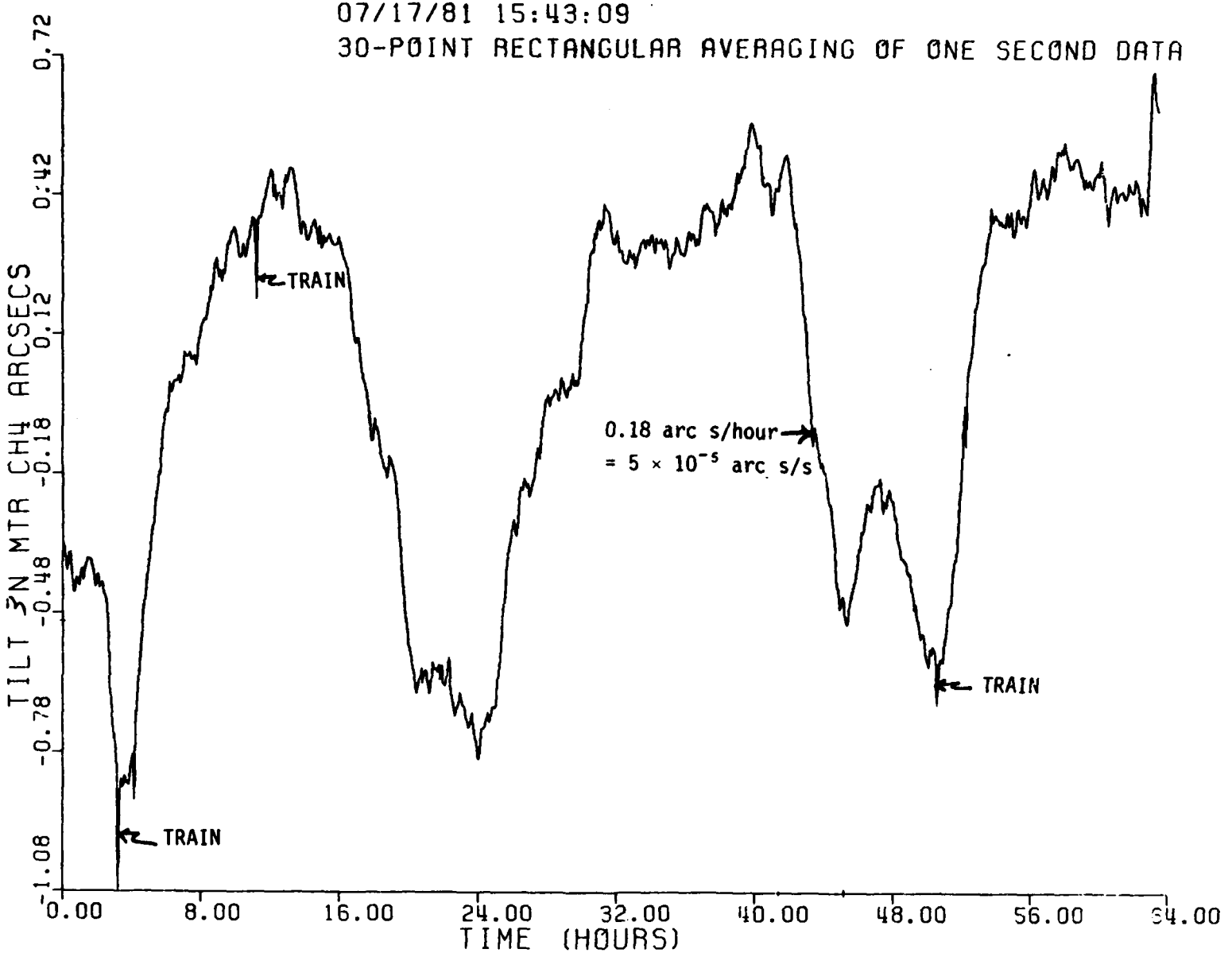

Figure 1. Tilt about east-west.

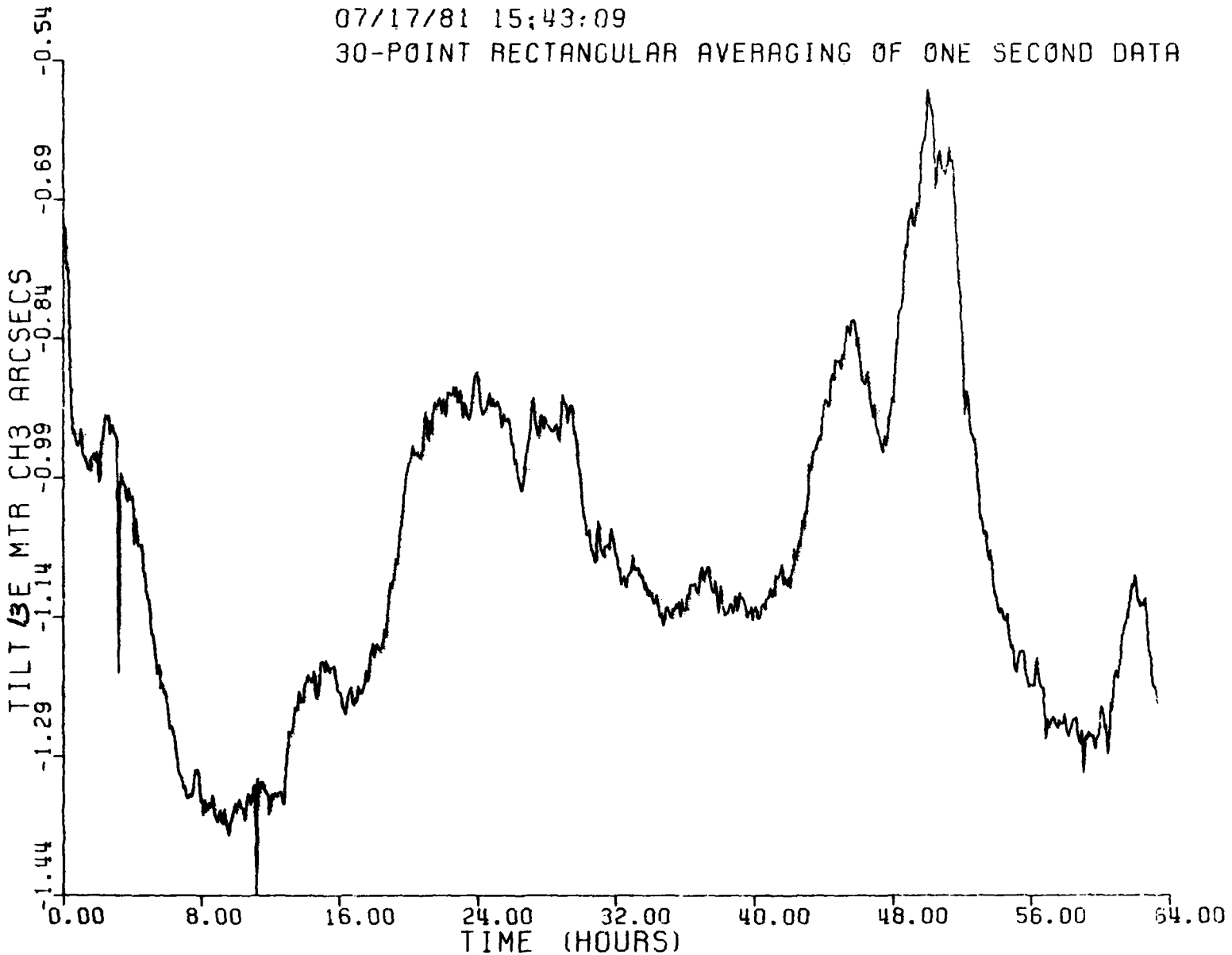

Figure 2. Tilt about north-south.

The tilt characterization segment showed that significant motions of the test station do occur which must be compensated for during gyro testing. Tilt rates about the gyro input axis (IA) approximately 0.18 arc s/hour (5×10^{-5} arc s/s) over some 8 hours were observed during several weekend runs. These rates were associated with diurnal temperature variations. Tilts were observed about both the north-south and east-west orientations.

Several trains which regularly pass nearby CSDL also generate ground motions which affect the test station. These events were detected by the tiltmeters as marked in Figure 1. Software for interpolating across bad data resulting from train motions was developed and implemented. A train detector was also installed to automatically mark these events. However, the detector was damaged during construction activity shortly after its installation and an accurate record of train activity was not available for most of the test program.

For the purpose of this analysis, a range of uncertainty from 0.002 to 0.005 arc seconds was assumed as the tiltmeter resolution at frequencies less than 1 Hz. For unfiltered data, the estimated uncertainty of the mean tilt signal over a one hour sample interval with a sample rate of 10 seconds would then be

$$\sigma_{\bar{\beta}} = \frac{\sigma_\beta}{\sqrt{n}} = \frac{0.005}{\sqrt{360}} = 0.26 \text{ m-arc sec}$$

The actual tilt uncertainty was much greater than this estimate, however. Tilt measurements from two co-aligned tiltmeters often deferred by as much as 0.2 arc seconds over any given 1-hour period (see discussion in Section 4.8). Assuming an error of 0.1 arc seconds from their mean as the actual error, the azimuth error due to tilt measurement errors could be as large as

$$\sigma_{\alpha_{\bar{\beta}}} = \frac{\omega_{erv}}{\omega_{erh}} \sigma_{\bar{\beta}} = 0.09 \text{ arc seconds}$$

Tilt rate can be defined as the angular rate sensed by the gyro input axis over the complete sample interval. Since tilt rate is not directly measurable, it is difficult to integrate all of the instantaneous rates throughout the sample interval. As an alternative, the net tilt rate over the finite sample interval can be determined by measuring the instantaneous tilts about the gyro IA (E-W) at the beginning and end of the sample interval and dividing by the sample duration, or by averaging multiple estimates over smaller increments throughout the sample interval.

As a practical matter, two additional factors influence the ability to measure instantaneous tilt. First, tiltmeters measure both tilt and horizontal accelerations, the two being inseparable in the tilt signal. Second, because of the filtering process necessary to reduce signal noise, the best estimate of instantaneous tilt is, in actuality, an estimated value determined from a smoothed tilt signal at the time of interest. The selection of tilt sampling and filtering is therefore bounded by these two considerations and the inherent instrument measurement error.

Typically, horizontal accelerations are found at frequencies higher than 1 Hz, while significant microseismic tilts occur at frequencies between 0.1 and 0.2 Hz. These conditions lend themselves to both analog (hardware) filtering and digital (software) filtering. A ten (10) second filter was applied to all tilt data by a common hardware filter in the tiltmeter power supply box. These data were then further triangularly filtered to 100 seconds by software and the average tilt rate over the 1 hour sample period was computed as

$$\bar{\omega}_{\gamma} = \sum_{i=0}^{360} \frac{T_{i+100} - T_i}{100 \text{ sec}}$$

Assuming a measurement uncertainty of 0.1 arc seconds for T_i, the tilt rate uncertainty is then estimated as

$$\sigma_{\bar{\omega}_\gamma} = \frac{\sigma_{\omega_i}}{\sqrt{n}} = \frac{\sqrt{\frac{2}{100}(0.1)^2}}{\sqrt{360}} = 7.5 \times 10^{-4} \frac{\text{arc sec}}{\text{sec}}$$

It should be noted that this is larger than the overall azimuth measurement error, since a rate (at full wheel speed) of approximately 5×10^{-5} arc seconds/sec will be interpreted as one arc second of azimuth deviation from true east.

4.2 Preliminary Gyro Evaluation and Preparation for WSM Tests

A series of alignment activities and short-term tests were accomplished as a prelude to WSM tests in order to evaluate the performance of the gyro at its normal wheel speed. These tests are listed in Table 1. Test durations ranged from overnight (16 hours) to over a weekend (70 hours).

Results from the preliminary gyro testing were well within the normal expected performance criteria. The uncertainty of the torque data was of the same order as the observed tilts, which suggested that the gyro would be acceptable for WSM testing.

One nagging problem did develop during this phase, however. A standard wheel rundown test was attempted, which consists of starting and stopping the wheel in various orientations, and comparing the wheel rundown characteristics for each orientation. The wheel rundown test was only partially successful. The gyro wheel was repeatedly started in the spin-axis-down position, but would not start with the spin axis up. Further, the wheel would not attain synchronous speed when started. However, the lack of synchronization was attributable to the frequency mismatch of the test wheel supply and gyro, and did not occur when the station wheel supply was used later in the test program. The restart problem did occur later in the experiment and precluded some desired testing.

Table 1. Preliminary Gyro Evaluation and Preparation for Wheel Speed Modulation Tests

1. Level 2-axis stand to table 360° reading.
2. Mount test gyro in stand.
3. Gyrocompass OA vertical to determine azimuth of table base.
4. Adjust table base to minimize azimuth error.
5. Mount PM-1 in place of test gyro.
6. Measure SG null and rotational stops.
7. Adjust quadrature and measure suspension phase angles.
8. Obtain overnight drift run OA ↑ -wheel off.
9. Check IA suspension polarity when wheel starts.
10. Check SA suspension polarity with rate about OA.
11. Check SG polarity with IA-North-open loop.
12. Check torque polarity with IA-North-closed loop and then South to obtain scale factor.
13. Align about SA and rough align about IA.
14. Measure 4 position unbalance and flotation OA//EA-N.
15. Measure axial flotation and bellows integrity OA up and down.
16. Perform wheel rundown test in 4 cardinal orientations.
17. Perform 4 position gyrocompass test to check azimuth and misalignment about OA.
18. Steady state drift - IA east to check torque stability.
19. Steady state drift - IA north, IA south to check scale factor stability.

4.3 Steady State (Fixed Position) WSM Tests

With the gyro IA "fixed" in a given orientation, the wheel speed was modulated between full and half speeds or full and quarter speeds once each hour (2 hours per complete cycle) for several days at a time. Tilts, temperatures and numerous gyro performance parameters described in Section 2 were monitored. Average tilt and tilt rate corrections were computed for each one hour average torque sample. The WSM azimuth was computed with and without compensation for tilt and tilt rate.

Two computational schemes were used for azimuth. First, a straightforward estimate was computed by differencing each successive one hour estimate at each speed according to the WSM model equation. Alternately, a three-point running average was also employed to reduce any phase errors associated with the 1 hour time difference between the means of the full and half speed torques. The three-point scheme averaged two like samples of torque (say two 1 hour samples at full speed, thereby matching the time of the half speed sample), and then computed the torque difference from full to half in the standard fashion. Similarly, the average of two half speed samples was then combined with a full speed sample, and the process continued iteratively.

Three point azimuth estimation typically reduced the long term uncertainty and is recommended for future processing.

Azimuth estimates obtained during fixed orientation WSM tests varied substantially according to the levels of environmental inputs. During quiescent periods, WSM azimuth uncertainties were usually less than 1.5 arc seconds following compensation for tilts and tilt rates. However, during "noisy" periods, azimuth uncertainties were often as large as 7-10 arc seconds. Typical corrections for tilt and tilt rates ranged from 0 to ± 2 arc seconds over a given 3 day interval.

Figures 3-6 show full-to-half WSM data from a sample overnight run where environmental variations were relatively small. The uncompensated azimuth uncertainty of a one hour estimate is 1.99 arc seconds (RMS uncertainty of a single observation during the 24 hour segment). When compensated for tilt and tilt rate errors (Figures 4 and 5), the uncertainty was reduced to 1.3 arc seconds (Figure 6).

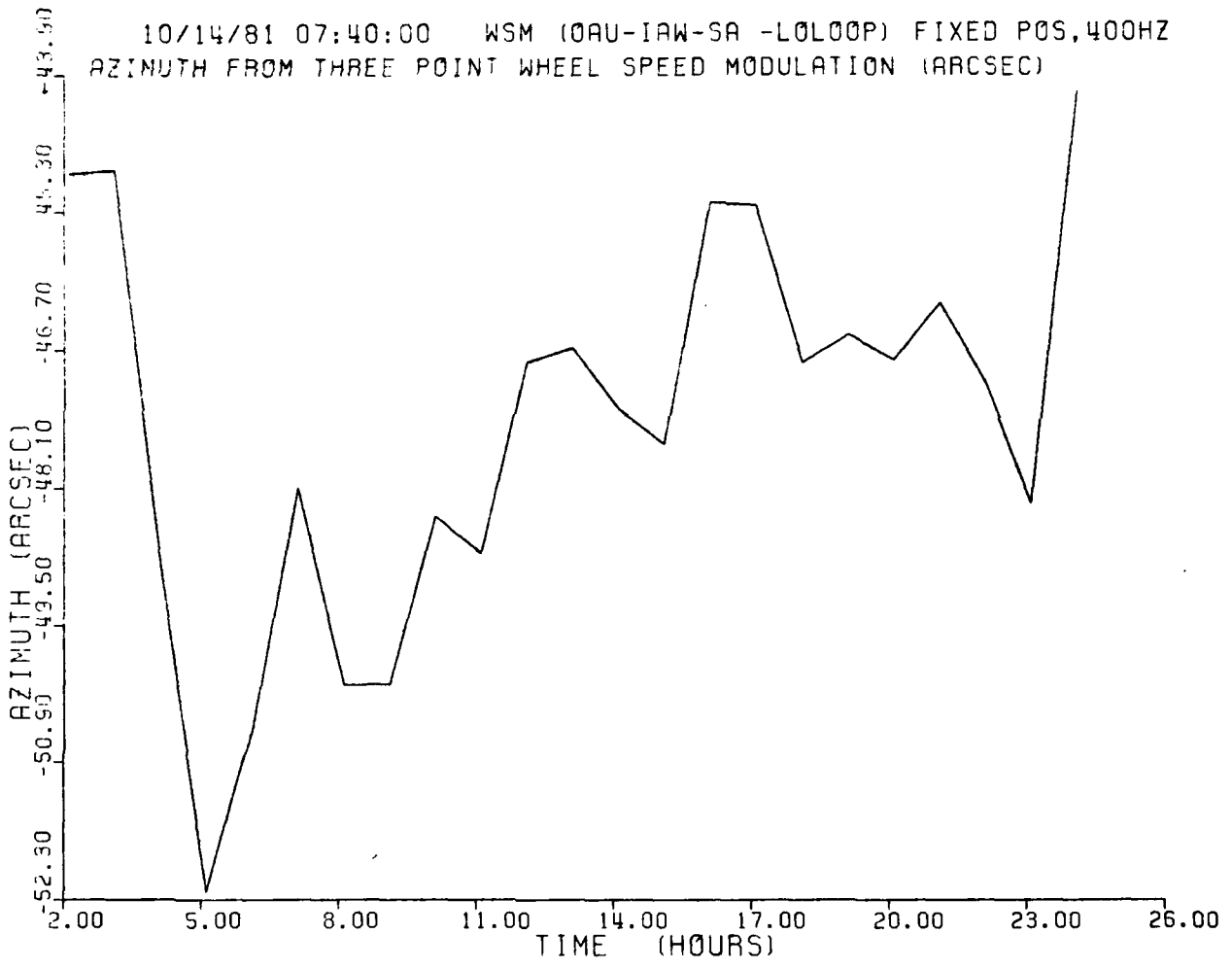

Figure 3. Uncompensated Azimuth from Full/Half WSM During Quiescent Overnight Run.

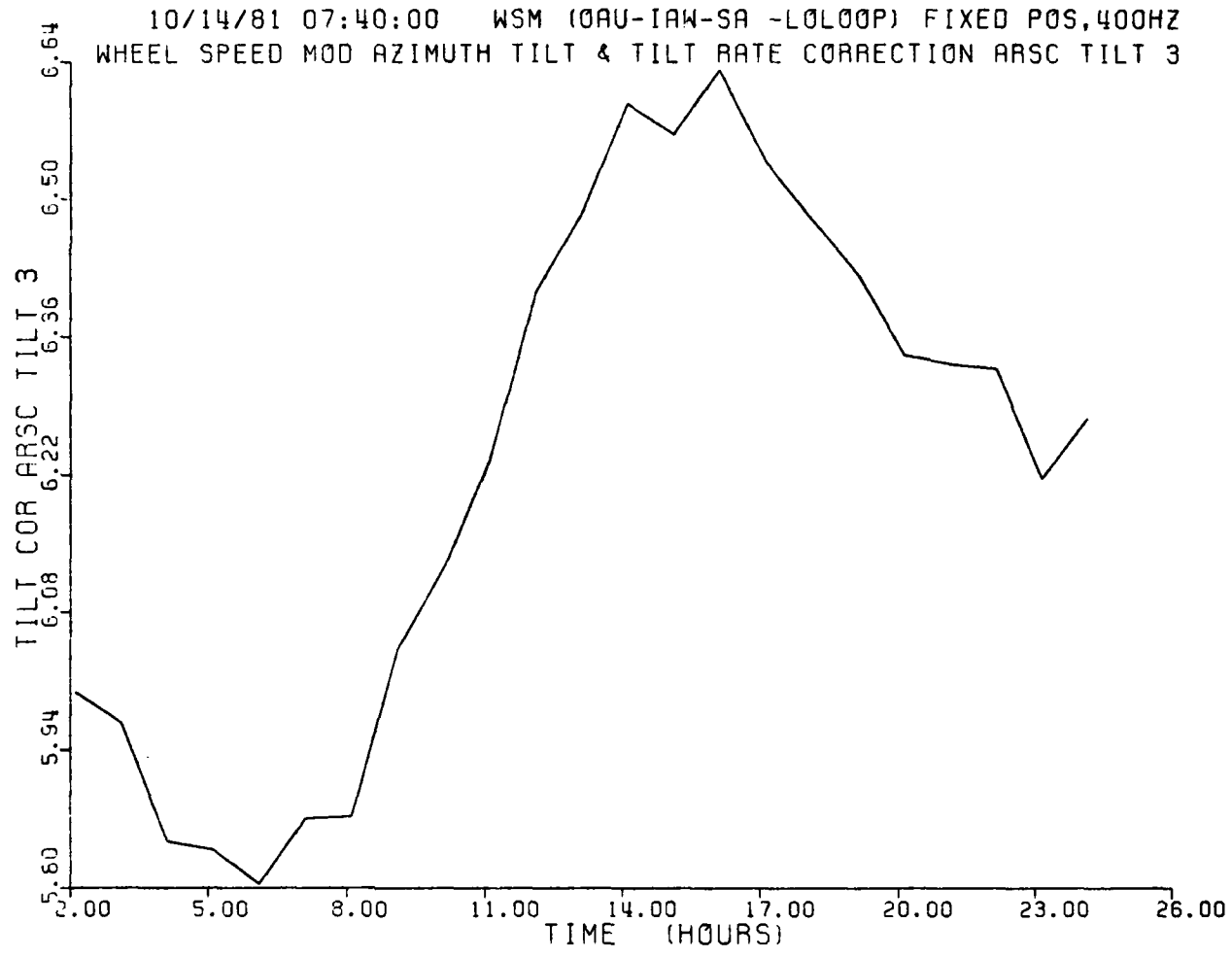

Figure 4. Tilt Compensations for Azimuth Data in Figure 3.

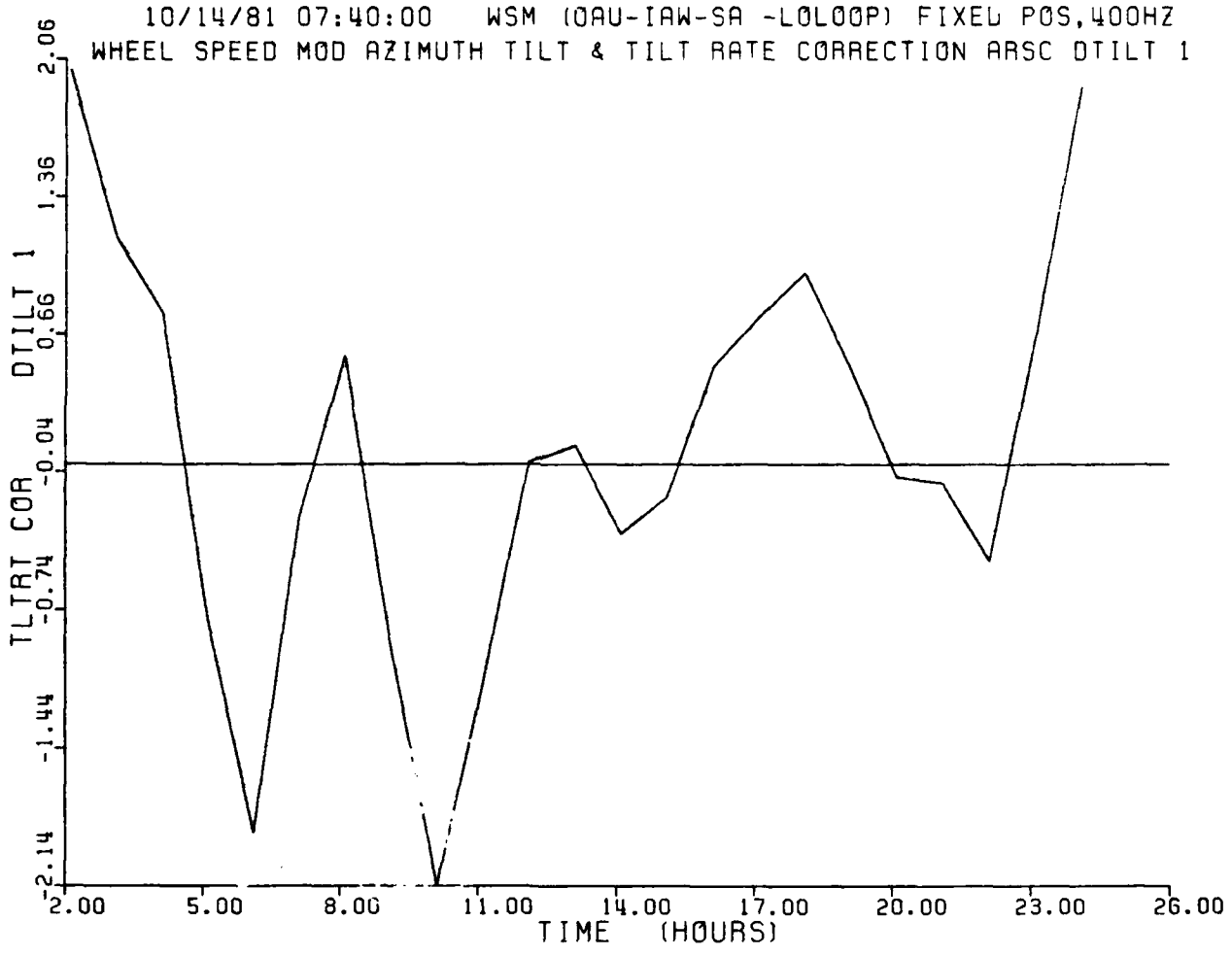

Figure 5. Tilt Rate Compensations for Azimuth Data in Figure 3.

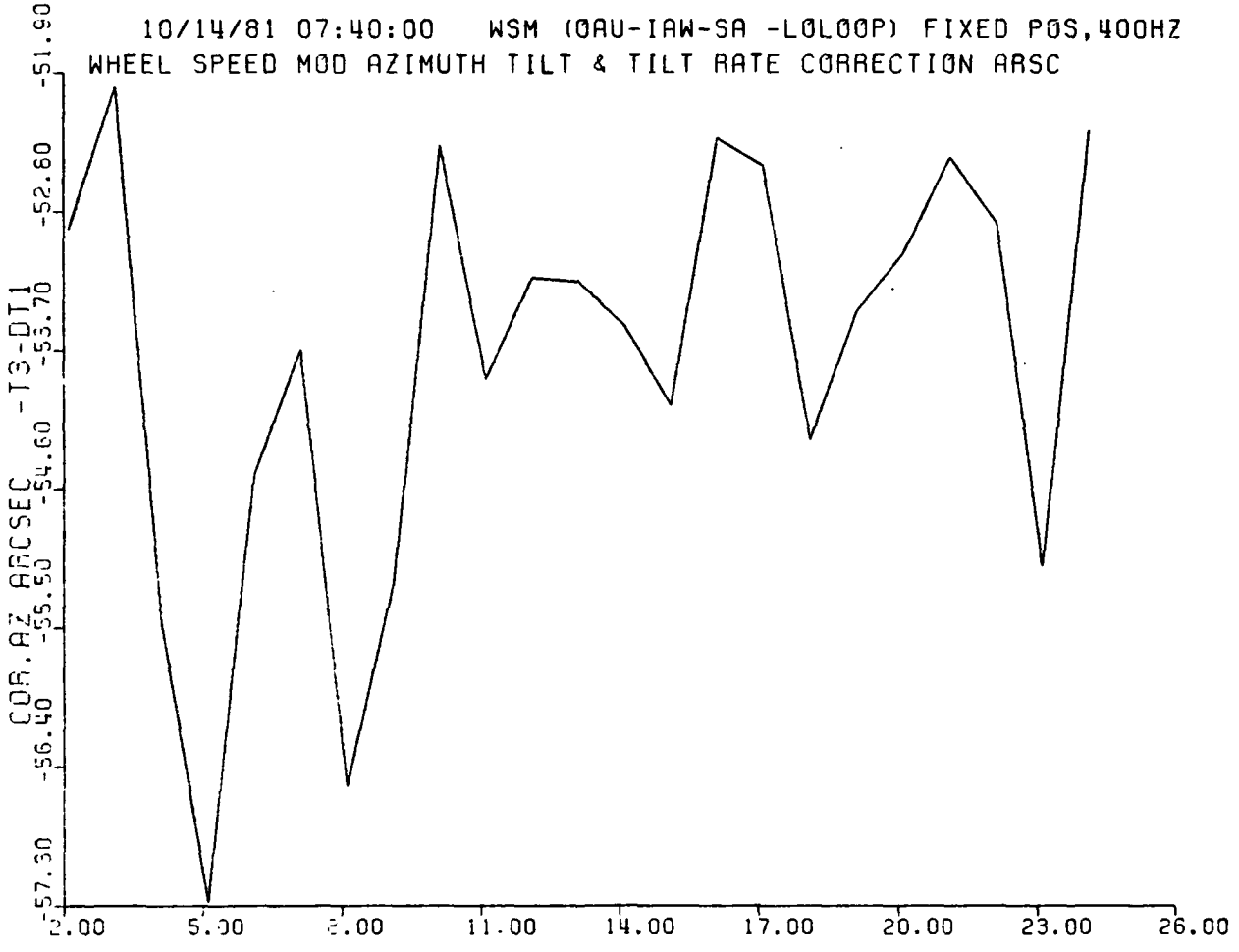

Figure 6. Compensated Azimuth from Full/Half WSM During Quiescent Overnight Run.

Figures 7-10 show data from a typical 3-day run of full-to-quarter WSM, where the environmental variations were again small. The uncompensated azimuth uncertainty (Figure 7) of a one-hour estimate is 0.76 arc seconds (RMS uncertainty of a single one-hour observation from the 66 hour mean azimuth). In this case, compensation for tilt (Figure 8) reduced the uncertainty slightly to 0.75 arc seconds, while compensation for tilt rate (Figure 9) increased the uncertainty to 0.88 arc seconds. This increase is probably attributable to the large measurement uncertainty of the tilt.

The low value of RMS uncertainty (0.76 arc seconds) for this and similar full-to-quarter WSM data segments readily demonstrate the capability of the PM gyro to measure azimuth with a repeatability below an arc second over extended periods of time. Since azimuth variations are actually occurring during these periods, and these azimuth motions are incorporated in the estimates of uncertainty, one can conclude that the measurement repeatability of the gyro is even better than the RMS uncertainties indicate.

These data also confirm the stability of $\Delta_K D_F$ during wheel speed changes to within the level of concern for WSM azimuth measurement.

4.4 Gyrocompassing with WSM

During this test sequence, the gyro was operated in each of the traditional gyrocompassing orientations with OA up and down and IA east and west at full and half wheel speeds for approximately 3 days each. From these data, misalignments of the gyro float with respect to case, mass unbalances, and average station azimuth and steady state gyro torque uncertainties were determined.

This test also satisfied a basic objective of comparing absolute (true) azimuth as determined by WSM with azimuth determined by traditional gyrocompassing. Agreement of the mean azimuth as determined by both techniques, coupled with the sub-arc second repeatability demonstrated during the full-to-quarter WSM tests, would then affirm the true azimuth measurement performance of the PM gyro using WSM.

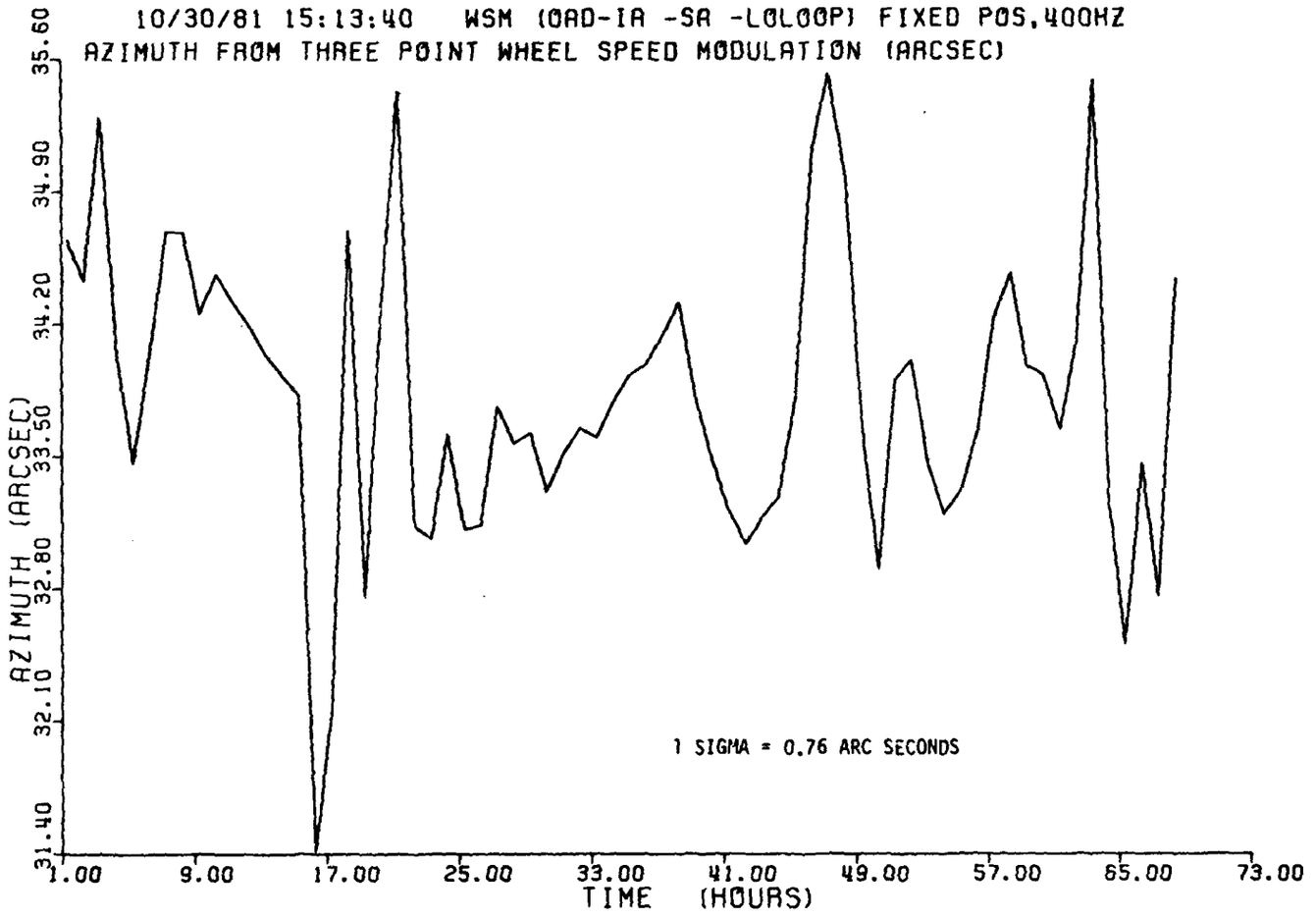

Figure 7. Uncompensated Azimuth from Full/Quarter WSM During Quiescent Three-Day Run.

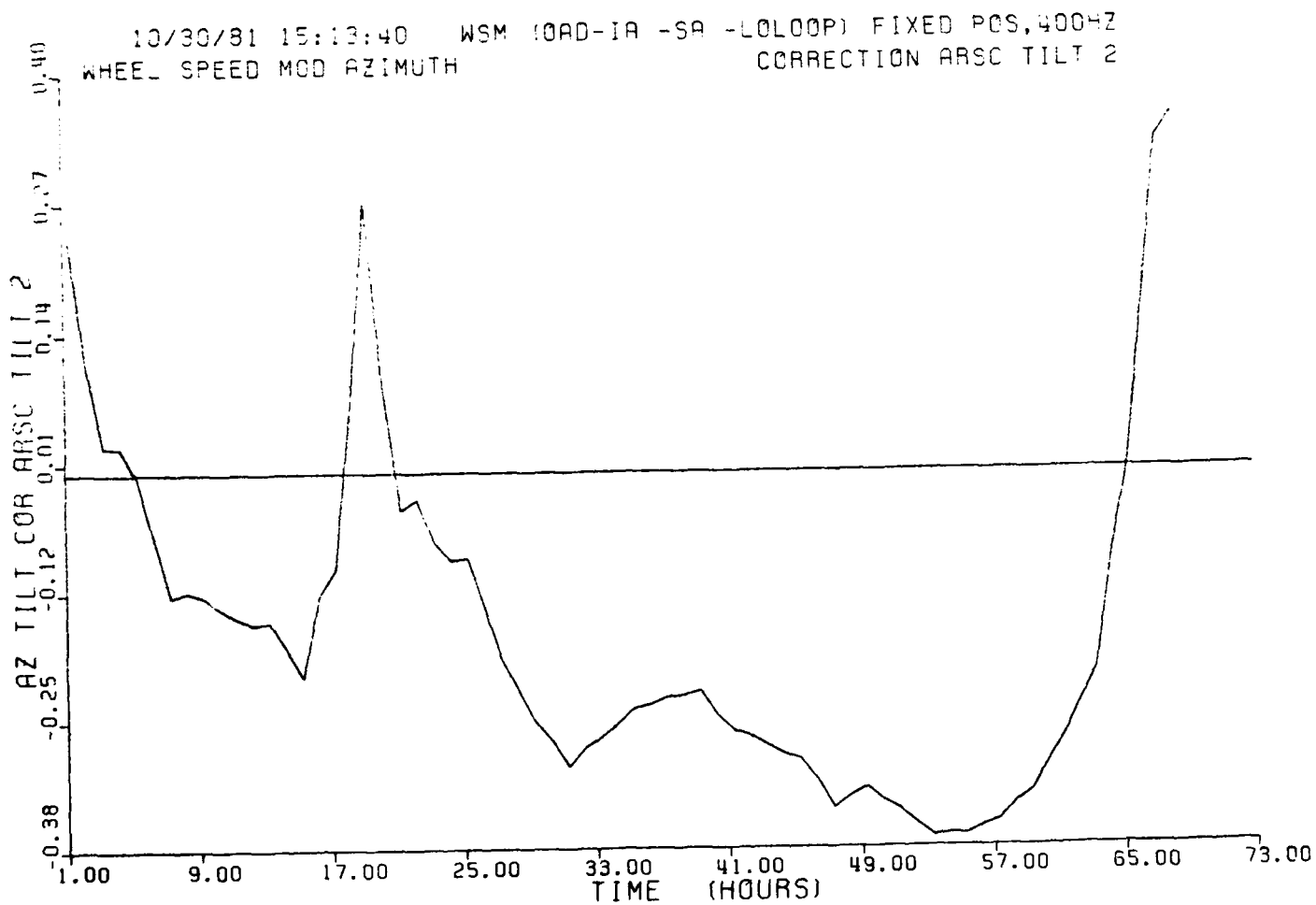

Figure 8. Tilt Compensation for Azimuth Data in Figure 7.

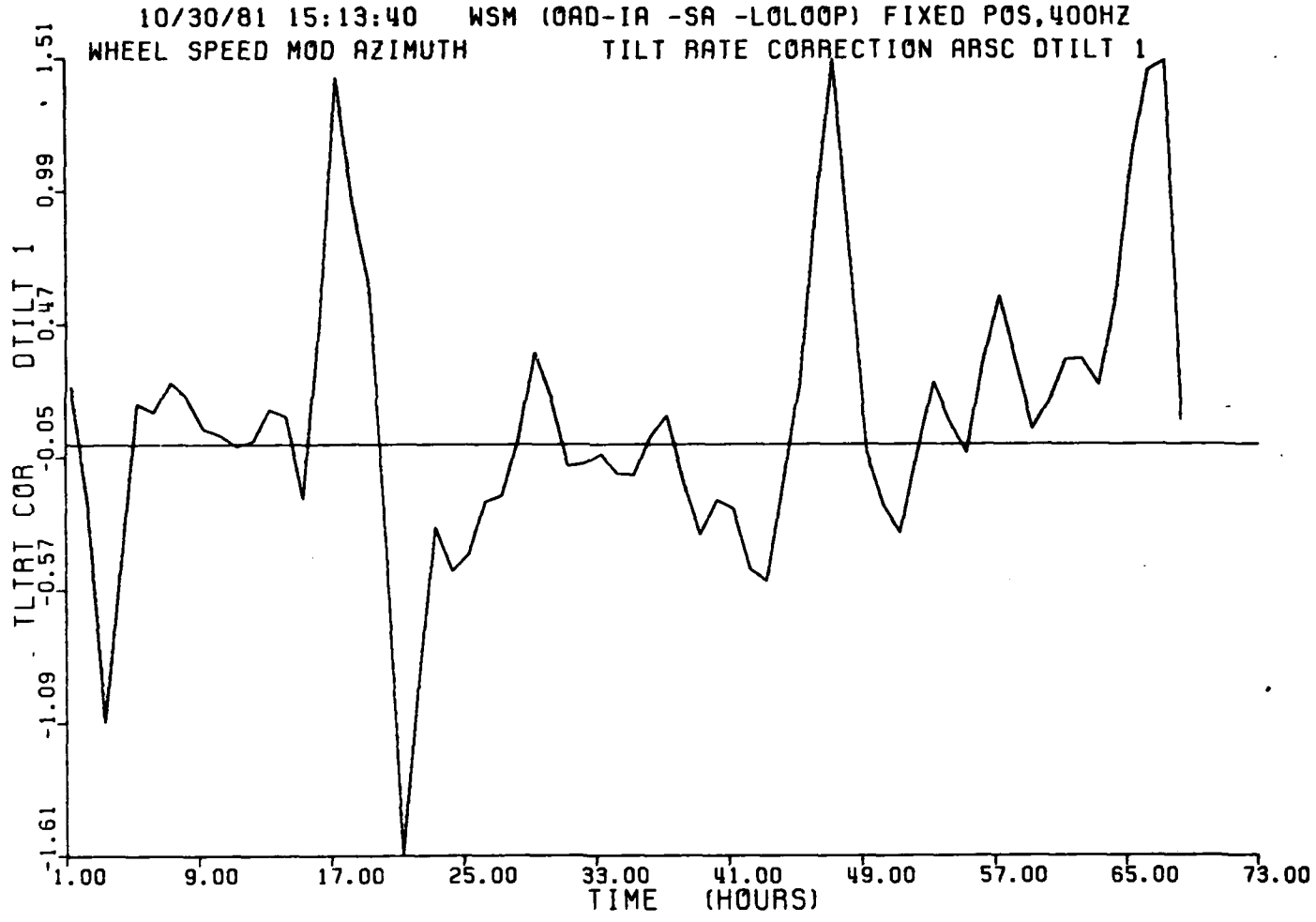

Figure 9. Tilt Rate Compensations for Azimuth Data in Figure 7.

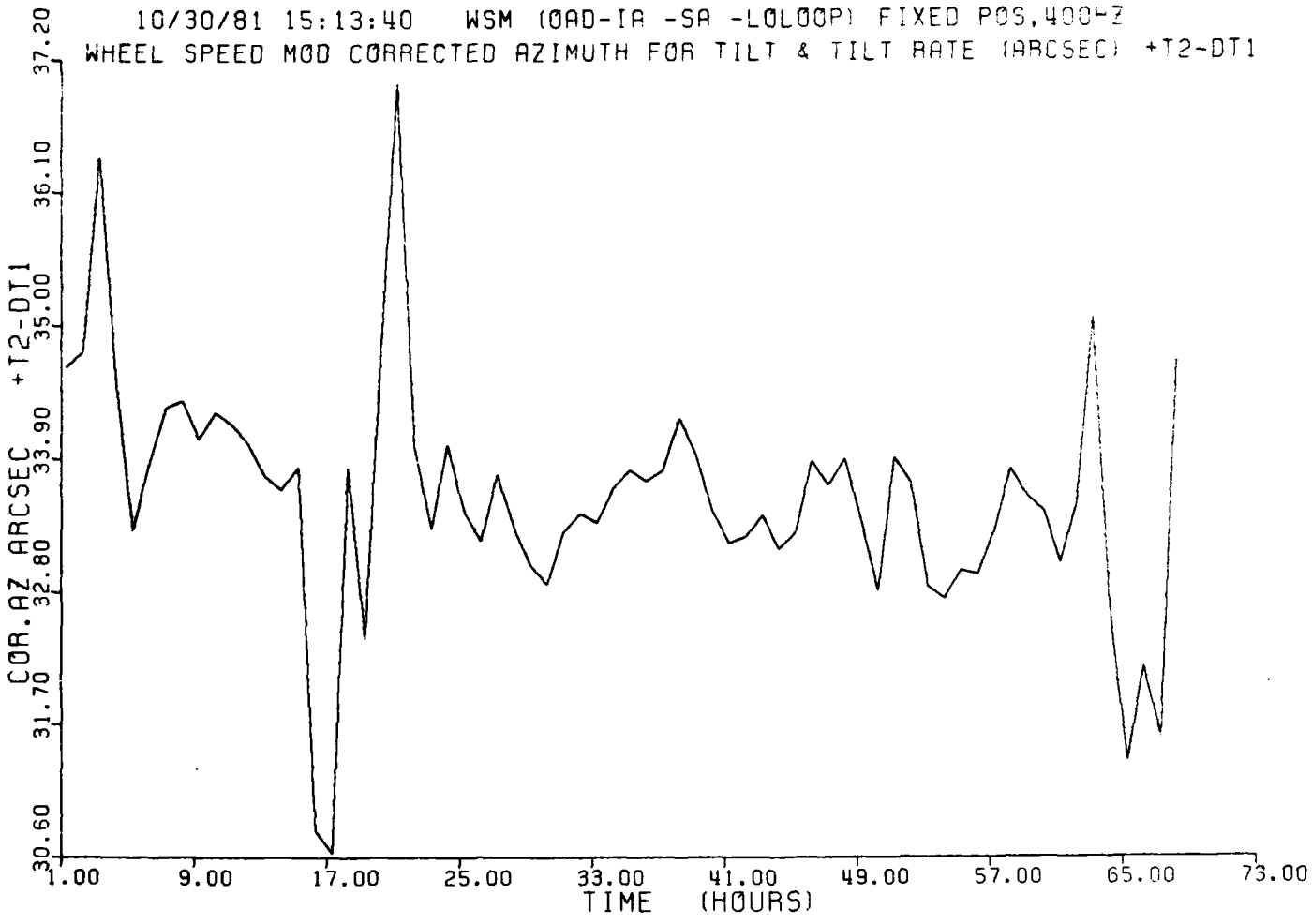

Figure 10. Compensated Azimuth from Full/Quarter WSM During Quiescent Three-Day Run.

The selection of a 3-day test interval for each of the four orientations minimizes the effects of very long-period azimuth trends (up to 10 arc seconds/year), and of short period variations (up to several arc seconds in the band between 3 to 24 hour periods) which tend toward a constant mean. Thus, the mean torques at the four orientations from both full and half speeds, were used to determine azimuth by gyrocompassing. These azimuth estimates from gyrocompassing were then compared with the mean WSM-determined azimuth for the entire test period to evaluate the true azimuth measurement capability using WSM. The torque uncertainties at each speed were also compared for the four orientations to further assess $\Delta_K D_F$ repeatability across multiple wheel speed changes and the long-term stability of $\Delta_K D_F$.

It should be noted that torque data contain long period variations over the 3-day intervals. But these variations are common to both full and reduced wheel speed data, and their effects are negligible when torque data are differenced. This is one of the major advantages of using WSM instead of gyrocompassing to measure azimuth for extended periods.

The test results showed that the error effects of misalignments on gyro torque during WSM were quite significant and often subtle. For example, an initial comparison was made between the WSM azimuth estimates at each orientation without consideration of the gyro float-to-case misalignments and the average table tilt. The azimuth estimates appeared to vary randomly between the four orientations by as much as 130 arc seconds. The magnitude of these variations seemed quite large when compared with the misalignment angles which ranged from 20 to 45 arc seconds. Further, each of the misalignments contributed to the variability of the azimuth estimates. Attempts to sequentially compensate for the misalignment errors showed that there were no dominant error terms, which when compensated for individually, would yield a nearly correct azimuth estimate.

Observation of this phenomenon led to a detailed re-evaluation of the gyro performance model for WSM. This model development is presented in Appendix A. The effects of each error parameter on the WSM azimuth estimates are represented by the simulated data in Figure 9 of Appendix A. Figures 10 and 11 are samples of actual test data. These data indicate that there is a 19 arc second systematic, and as yet unresolved difference in the azimuth estimates between OA up and down which cannot be accounted for by compensation for constant misalignments. Although tilt effects were not considered in these data, later evaluation showed that they were not the cause of the unresolved errors.

The data in Figure 11 of Appendix A suggest that a "true" azimuth of approximately -16.6 arc seconds can be computed in each of the four positions by applying separate compensation for IA misalignment about OA at each wheel speed. Actual occurrence of this condition is unlikely, however, and the phenomenon warrants further investigation. Unfortunately, the limited performance period of this investigation did not permit repetition of the test with either full-to-half or full-to-quarter WSM.

4.5 Angle Measurement with WSM

The previous test, which combined WSM with gyrocompassing, provided a good estimate of how well the mean true azimuth could be measured with WSM. However, because each measurement interval was approximately three days long, short period azimuthal motions could not easily be separated from gyro instabilities. Thus, a special test, combining position modulation with WSM, was devised to attempt to remove any short term azimuth variations.

This test determined the difference between the azimuth estimates of two fixed orientations. Two rigid stops were fixed to the test table approximately one degree apart, so that the gyro IA was alternately pointed at approximately zero or one degree. The table was then iteratively positioned back and forth between the stops, while the gyro wheel speed was changed between full and half speed at each position. Thus, the azimuth of each position was continuously estimated by WSM each time the table was repositioned, and the included angle was computed from successive azimuth estimates.

Since some positioning error was possible as the table was moved from stop to stop, an autocollimator and two mirrors were used as a second vote to monitor positioning repeatability. Unfortunately, the autocollimator did not have a range large enough to measure the full range of the table motion. Therefore two separate signals were observed, one for each mirror corresponding to the two table positions. Despite the discontinuity between table positions, the autocollimator data indicated that the positioning error was usually less than several tenths of one arc second. However, there were intermittent periods when the table torquer did not hold the table tightly against the stops. This resulted in considerable measurement noise and position uncertainty.

The accuracy and repeatability of measuring the included angle was supposed to be a measure of WSM accuracy and of the repeatability of $\Delta_K D_F$, since the included angle should not change with time. But unfortunately, the results of this test were also masked by the effects of the environment (see discussion in Section 4.9). The mean WSM estimate of the angle from several days of continuous measurement did agree with the true angle to within 0.2 arc seconds. But the peak-to-peak WSM estimate varied from less than an arc second during the quieter periods to as much as 18 arc seconds during periods of increased tilt and temperature variations. Correction for tilts and tilt rates did not significantly reduce these large variations.

Data from a 42 hour test sequence are shown in Figures 11-15. Figures 11-12 show the respective azimuths at each table stop and Figure 13 shows their difference. Note that the included angle measurement is fairly repeatable except during the period from 16-28 hours. Figure 14 is the tilt about the gyro's north-south axis, and Figure 15 is the tilt rate about the east-west axis. Some of the error in the anomalous period can be accounted for by the tilt rate correction which is as large as 4 arc seconds. But this does not account for the majority of the error.

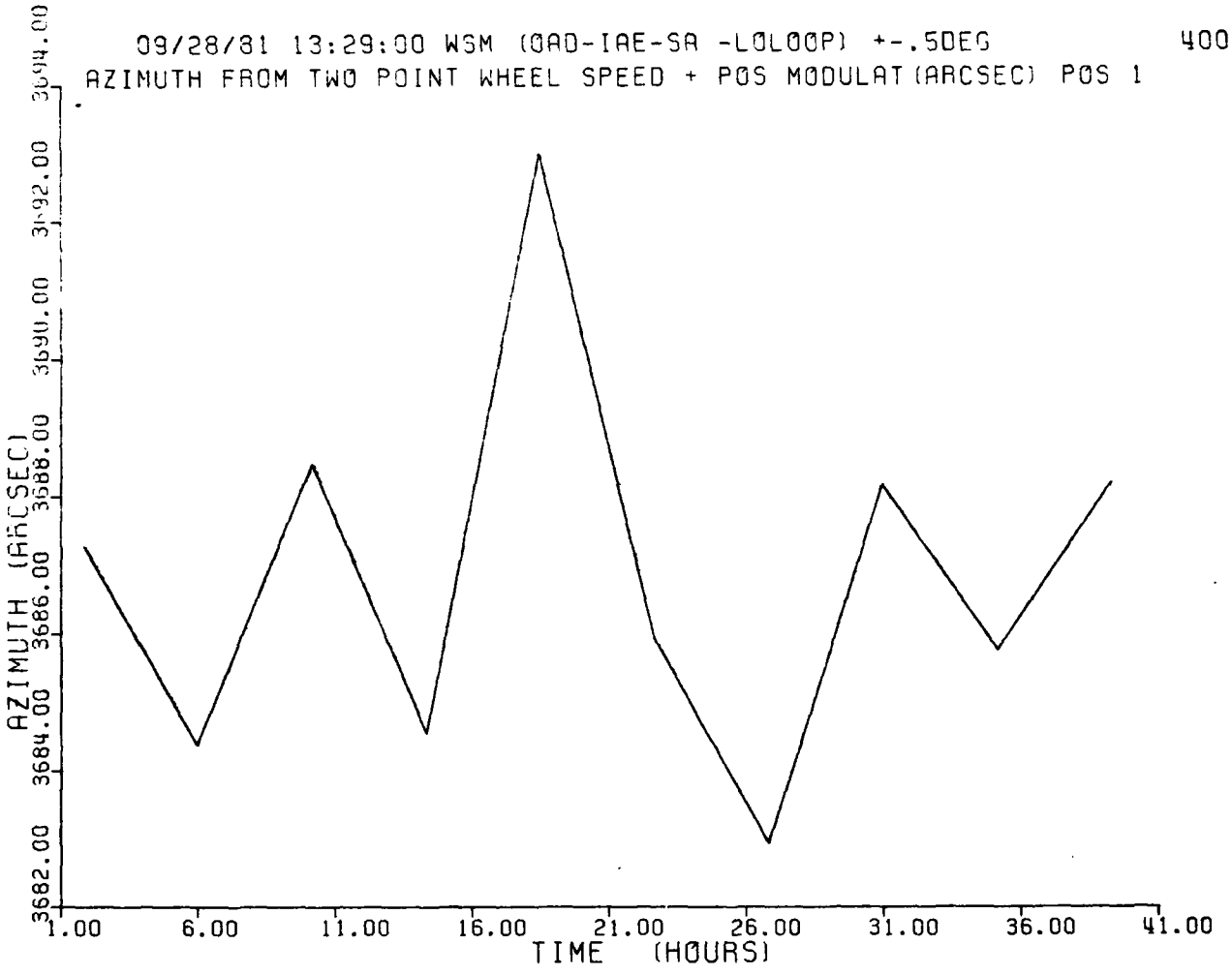

Figure 11. Full/Half WSM Azimuth of Test Table Position 1.

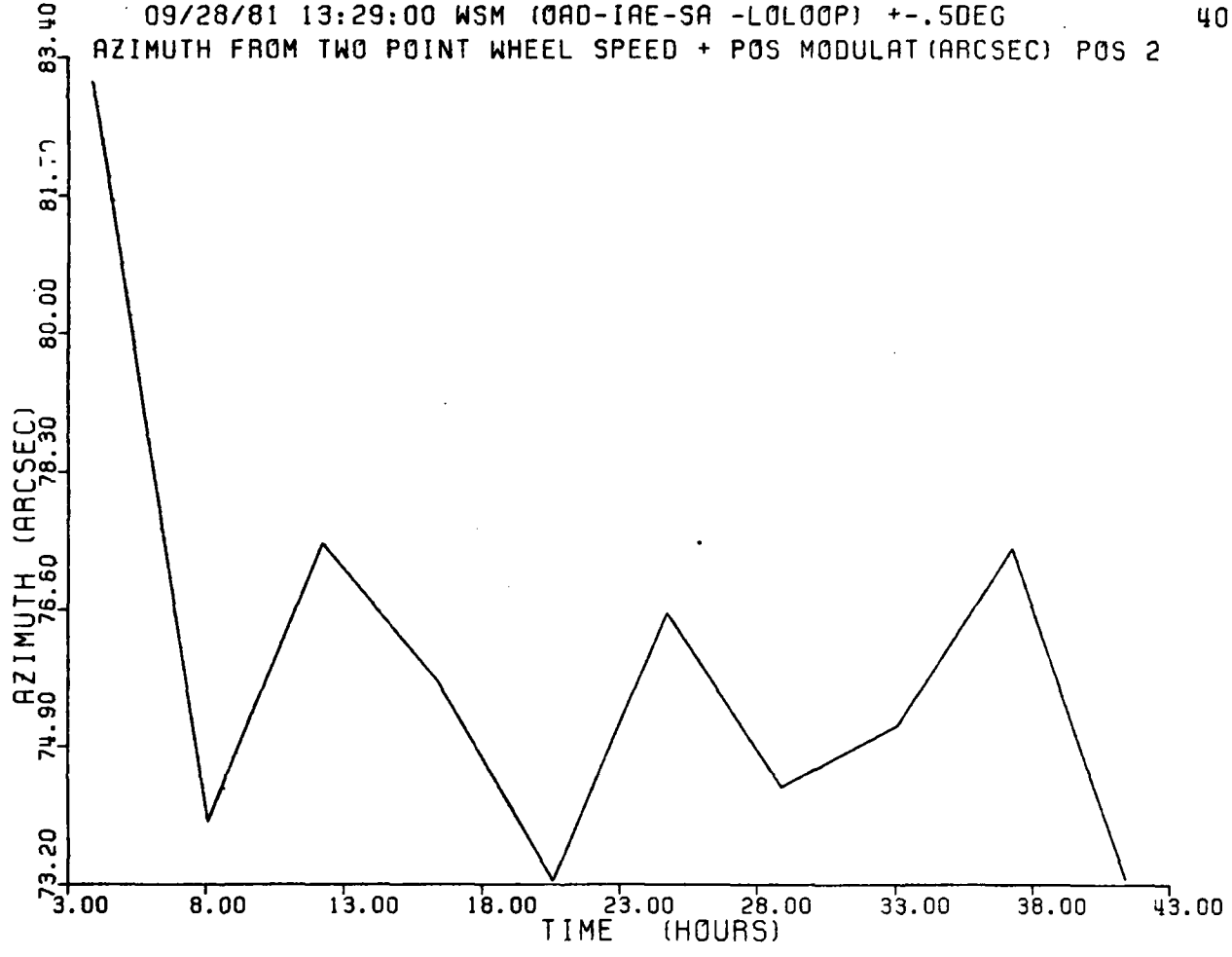

Figure 12. Full/Half WSM Azimuth of Test Table Position 2.

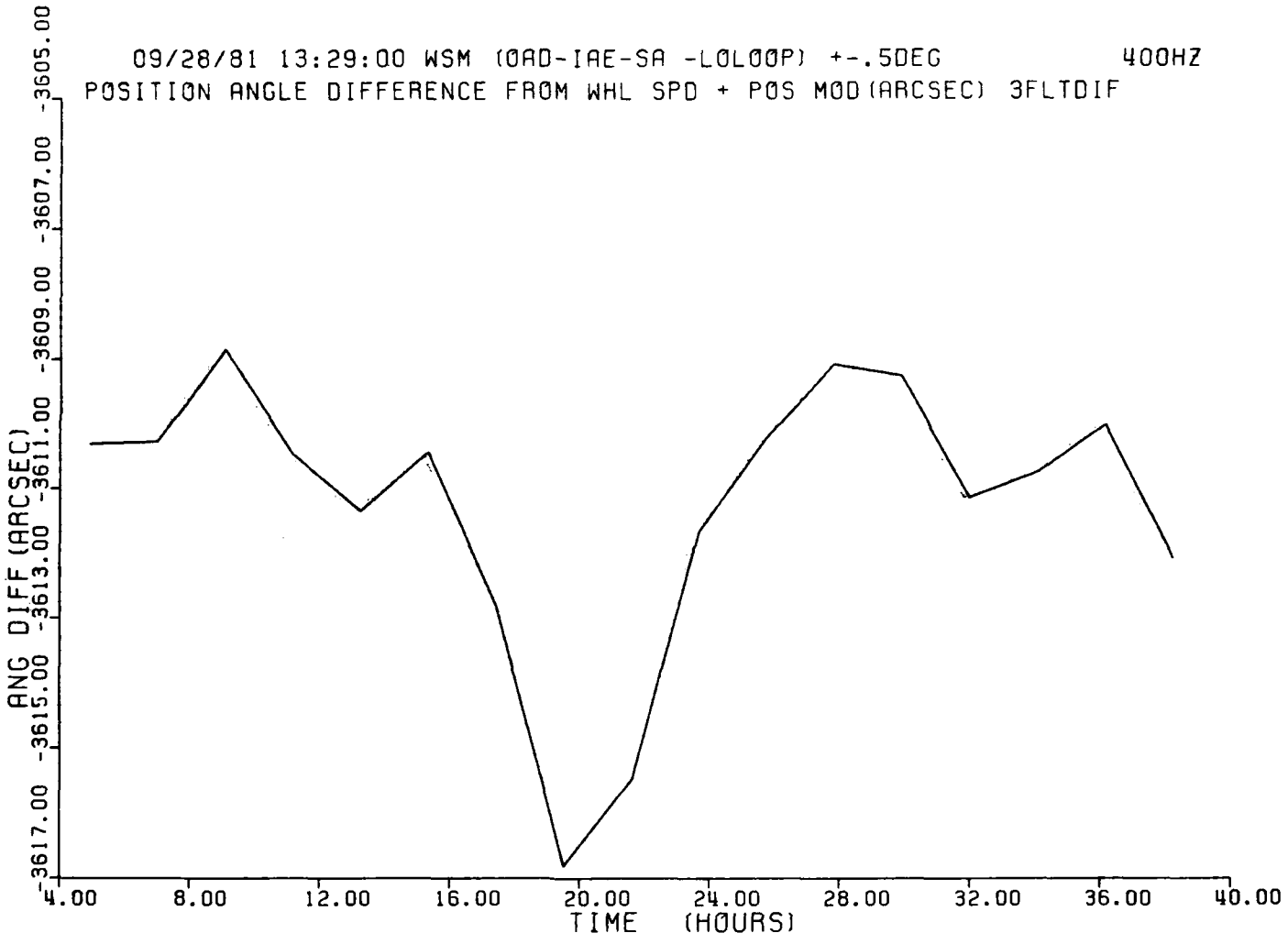

Figure 13. WSM-Determined Angle (Position 1 - Position 2).

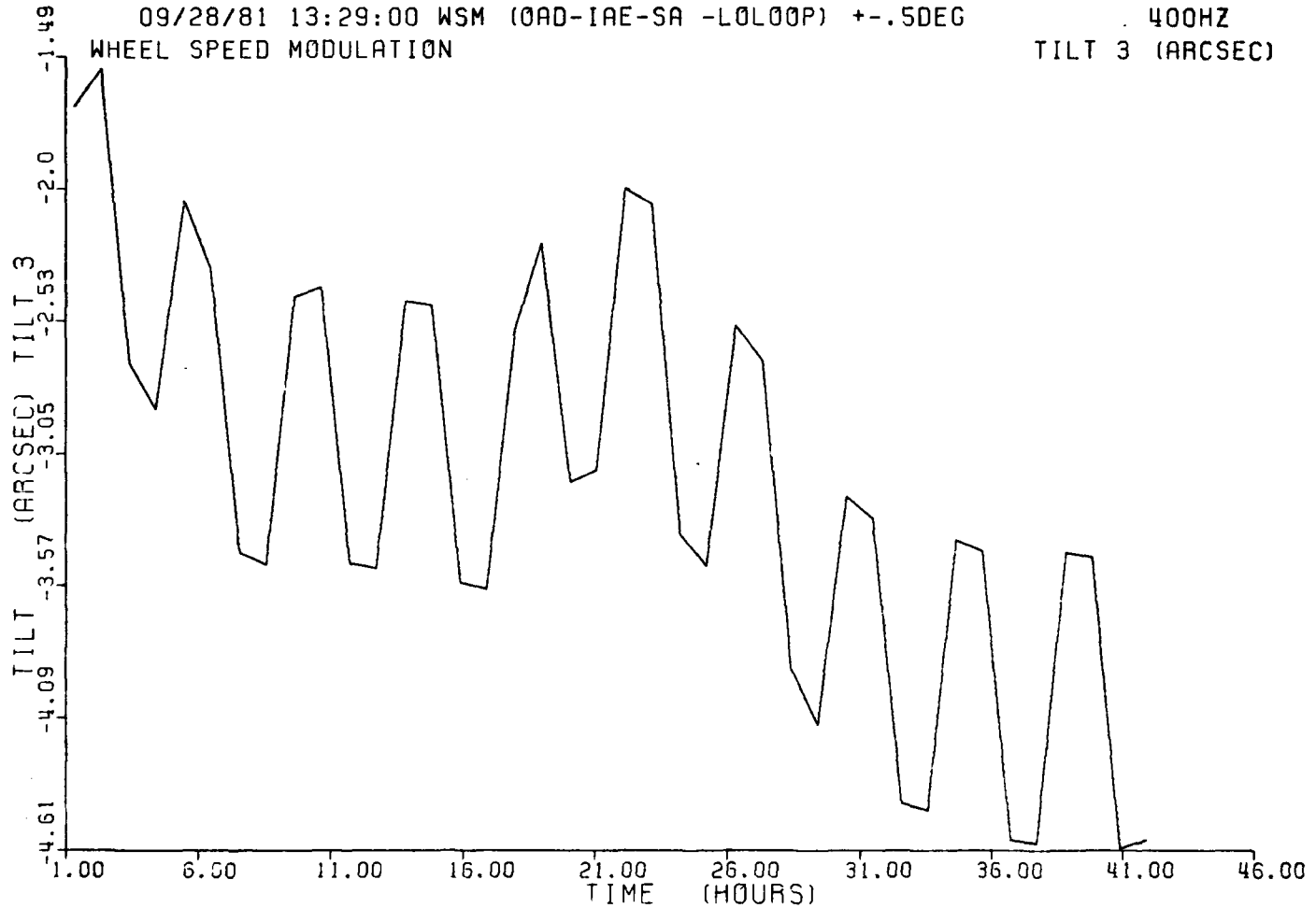

Figure 14. One Hour Average Tilts at Test Table Position 1 and 2.

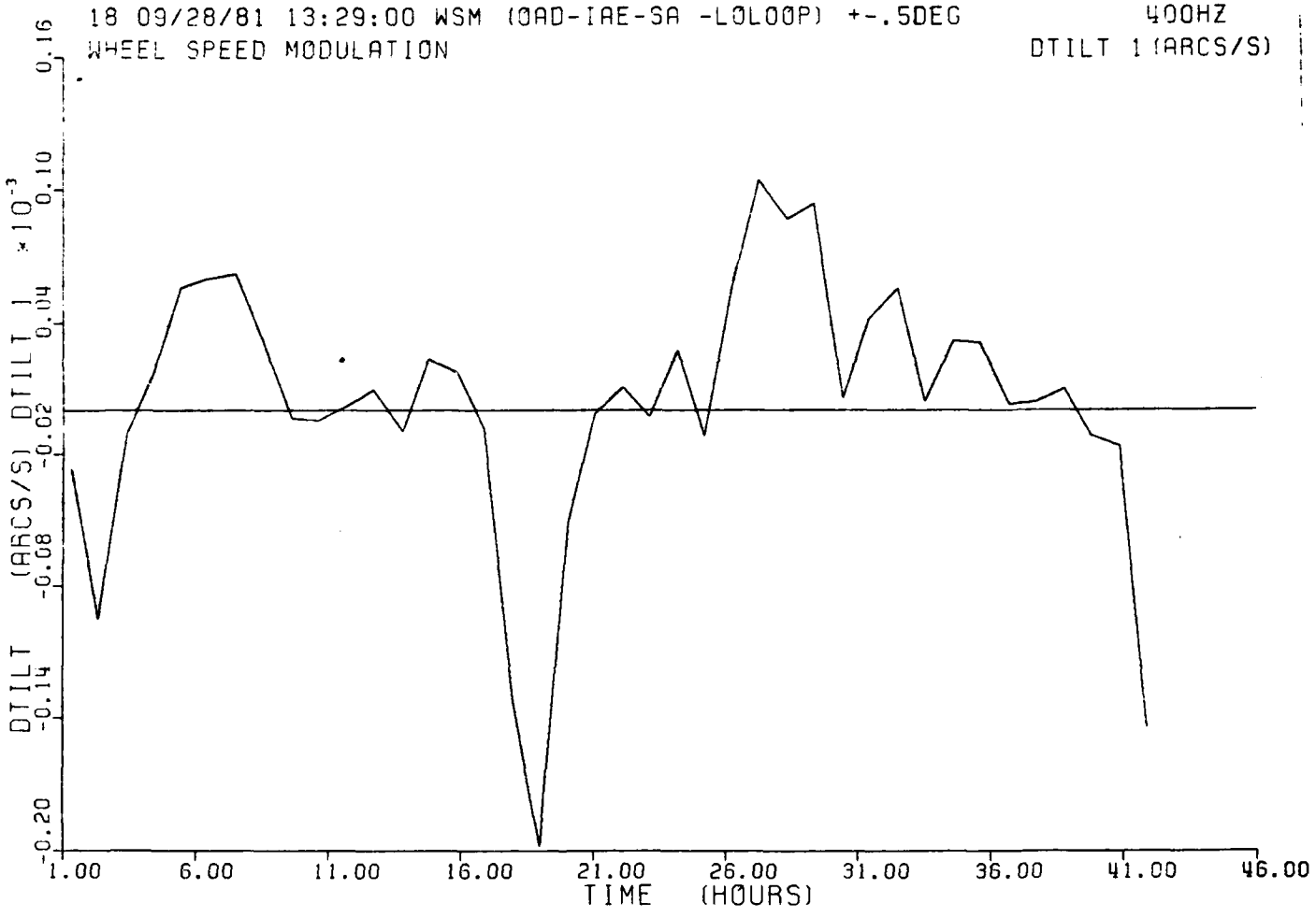

Figure 15. One Hour Average Tilt Rates at Test Table Position 1 and 2.

Figures 16-18show autocollimator and temperature data for a 69 hour test segment which includes the above period. The long term drift of position 2 indicated by the autocollimator does not show up in the gyro data so this is evidently a drift in the signal or gradual azimuth motion of the mirror surface and not the test table. The plot does show, however, that there are no drastic table motions which would cause the variations in angle shown in Figure 13.

Figures 17 and 18 are the ambient temperature inside the station enclosure, and the wall temperature in the test laboratory, respectively. These data suggest some autocollimator temperature sensitivity, but not enough to mask the evaluation of table position repeatability.

This test segment did contribute to the overall evaluation, despite the above difficulties. First, it confirmed that small angle changes of approximately one degree can be detected and accurately measured over extended periods of time. Second, it confirmed that $\Delta_K D_F$ does not change significantly with time. These two requirements are a necessary part of the successful use of a WSM gyro in an azimuth measuring system.

4.6 $\Delta_K D_F$ Repeatability Across Power Shutdown

The intended objective of this test was to evaluate the repeatability of $\Delta_K D_F$ across multiple power shutdowns which one might expect if the gyro were used in a portable azimuth measuring system. Because of difficulties in starting this particular gyro during the preliminary test sequence, this test segment was eliminated from the test program. However, one automatic shutdown did occur due to an abnormality in the gyro temperature monitor safety circuit. Since there were no distinguishable changes in any of the data across the shutdown, and restarting the gyro was again difficult, it was deemed inappropriate to risk a gyro wheel failure by performing multiple power shutdowns. Note that this condition is peculiar to this test gyro (probably due to bearing contamination), and is not a typical gyro characteristic associated with WSM.

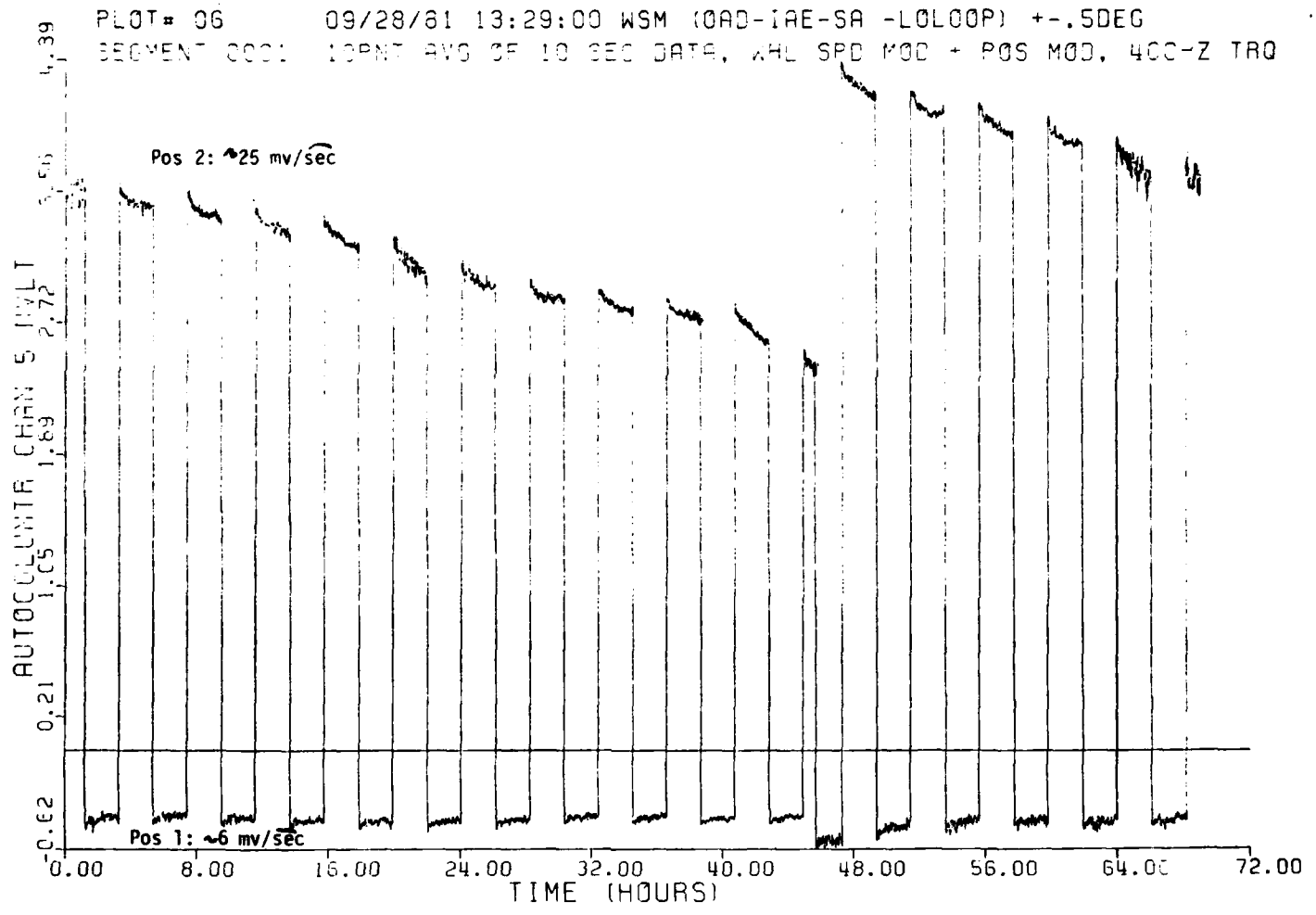

Figure 16. Autocollimator Signals at Test Table Positions 1 and 2.

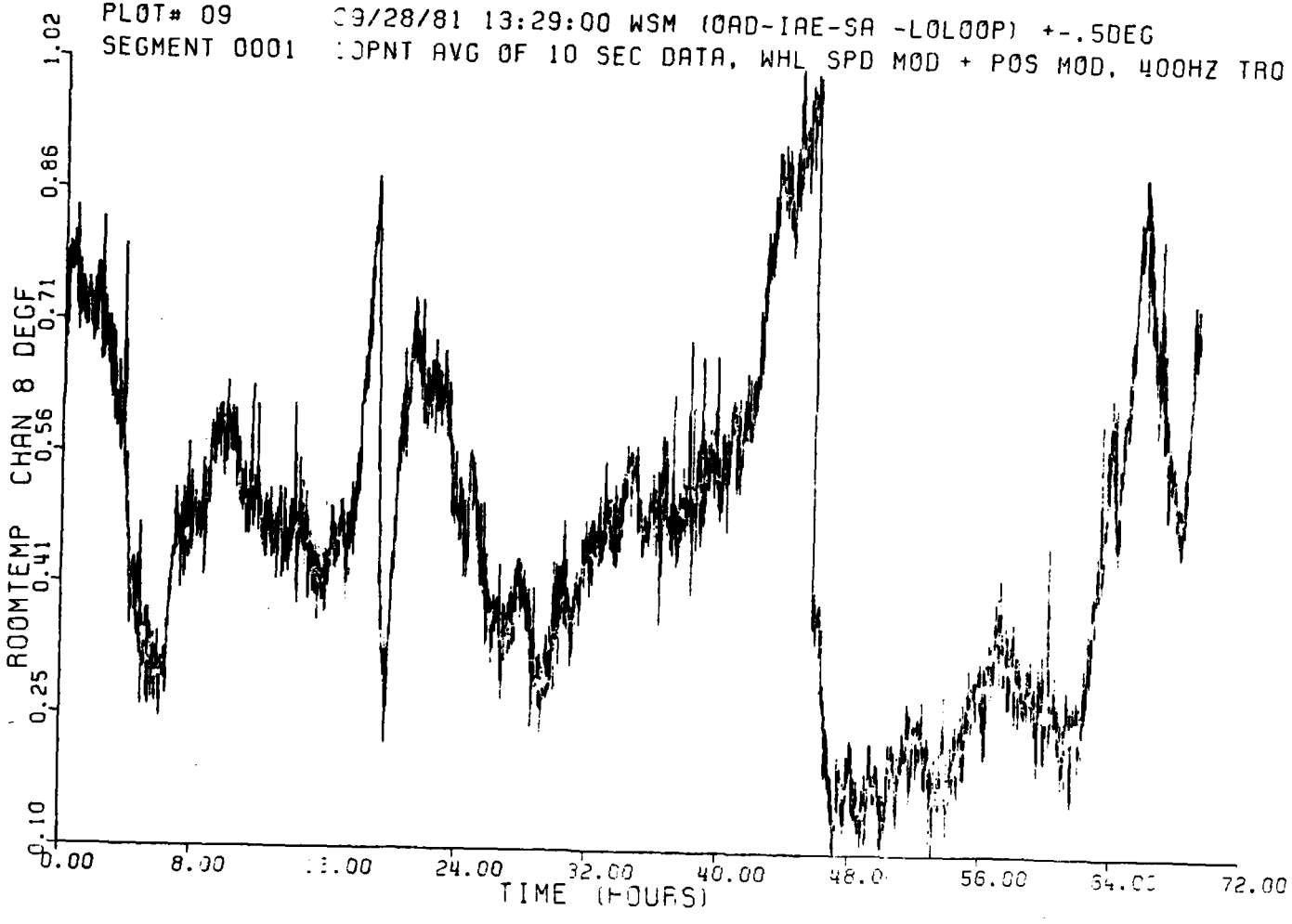

Figure 17. Room Temperature Corresponding to Figures 11-16.

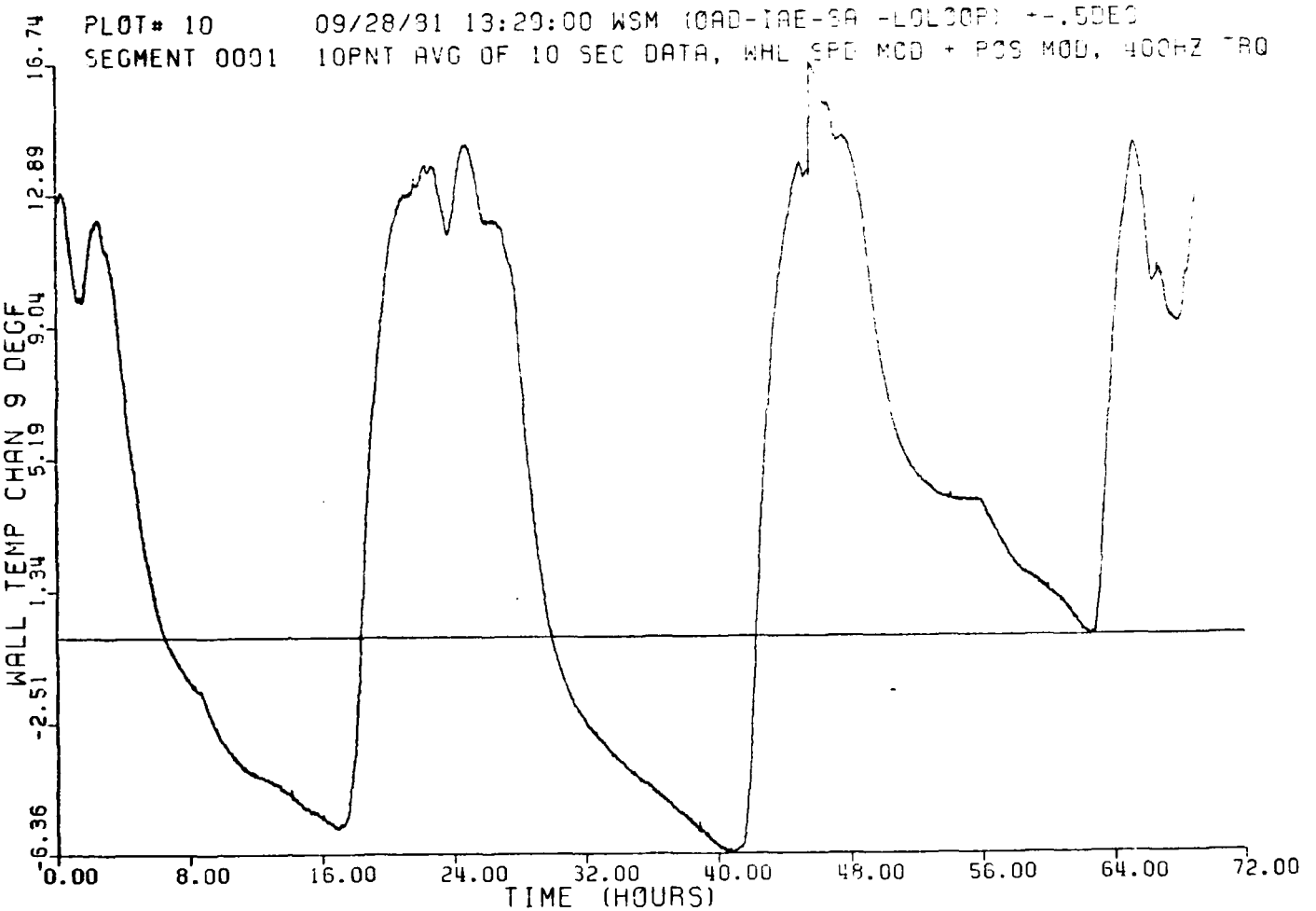

Figure 18. Wall Temperature Corresponding to Figures 11-16.

4.7 Evaluation of Reduced Wheel Speed Alternatives

Time did not permit a complete study of wheel speed optimization and transient modeling. Yet some insight into the effects of varying the reduced speed was obtained since many of the tests were performed using both full - to-half WSM and full-to -quarter WSM. In all cases, the first 15 minutes of the one hour steady-state gyro totque data were discarded to ensure that the data were not corrupted by speed change transients. This was probably very conservative, since Wheel power, heater power and torque transients were all no longer visible within less than 8 minutes after a speed change.

In general, there seemed to be no appreciable difference in the one hour torque uncertainties at any of the selected wheel speeds. Further, a short segment of data was collected with a 2 hour dwell period at each speed. This also had no effect on the repeatability of the torque data within each 2 hour sample period.

In contrast, there was a slight improvement in the azimuth uncertainty when using full - to-quarter WSM vs full - to-half WSM. However, even though these data were obtained during similar test configurations, there were often several weeks between the tests, thereby casting some doubt on the comparability of the test environment. A qualitative evaluation of the ensemble of the test data shows that the tilt and temperature variations were typically smaller during full - to-quarter WSM tests than during full -to -half WSM tests. This could be due to the fact that most full- to -half WSM tests were performed in August and early September when the day-to-night temperature extremes were greatest. Most full- to -quarter WSM tests were performed later when temperatures were not as extreme.

Finally, a 3 day test was run where a 5-minute intermediate change to 3/4 wheel speed was inserted between each full/half cycle. This test was designed to quickly evaluate the effects of speed changes on Output Axis (OA) float motion. OA float motion proved to be very repeatable, with amplitude quite linearly dependent on the change in wheel speed. This conclusion is very encouraging since float motion along OA induces gyro

error torques with a time constant of several hours. Variations in float motion would result in uncalibratable error torques which in turn would induce large azimuth uncertainty.

4.8 Environmental Effects on Azimuth Measurement During WSM

The occurrence of variations in environmental conditions seemed to cause directly correlatable, but unexpectedly large azimuth variations. Tilt cycles, usually associated with diurnal temperature cycles, caused erratic azimuth estimates, which were typically 4 to 5 times greater than the tilt/tilt rate compensation models predicted.

This phenomenon is exemplified by the 4-day data segment starting 10/09/81 shown in Figures 19-23. Figure 19 shows the WSM torque for the interval. Note the irregularities surrounding the periods between 3-9 hours, 25-31 hours, 49-57 hours, 72-78 hours and starting at 96 hours. Figure 20 shows the uncompensated WSM azimuth estimates for the same interval. Note the effects of the torque irregularities on the azimuth estimates. Figures 21 and 22 show the estimated tilt and tilt rate corrections to the WSM azimuth estimates. Although the motion corrections correlate exactly in time with the azimuth variations, they are of much smaller amplitude and are not sufficient to explain the large apparent azimuth fluctuations as shown in Figure 23.

Initially, the accuracy of the tilt measurements with the AFGL tiltmeters was considered to be a likely candidate for the unaccountable errors. There was often significant disagreement between tiltmeters which were located side by side and parallel to one-another. This disagreement was as large as three arc seconds across a 5-arc-second tilt event as exhibited in Figures 24-29.

The four tiltmeters were oriented in antiparallel pairs, with each pair measuring tilt in a cardinal direction. Thus, each tiltmeter in the pair should record equal but opposite tilts for each event, and their sum should be a constant value barring any long term tiltmeter drift. Figure 26 is the sum of the tiltmeter signals shown in Figures 24 and 25, Figure 29 is the sum of the signals shown in Figures 27 and 28. The

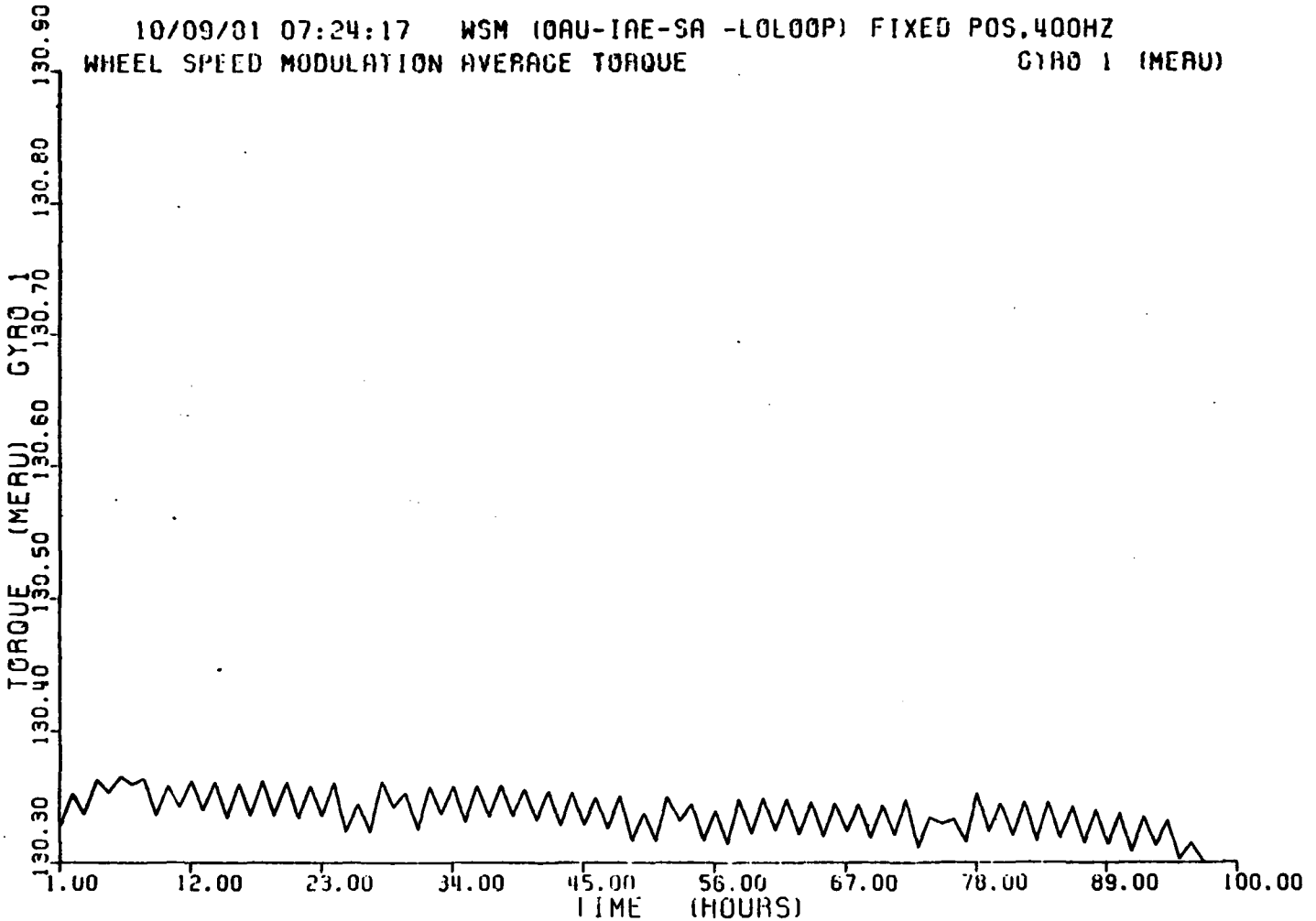

Figure 19. Full/Half WSM Average Torque for 4-Day Interval with Significant Environmental Influence.

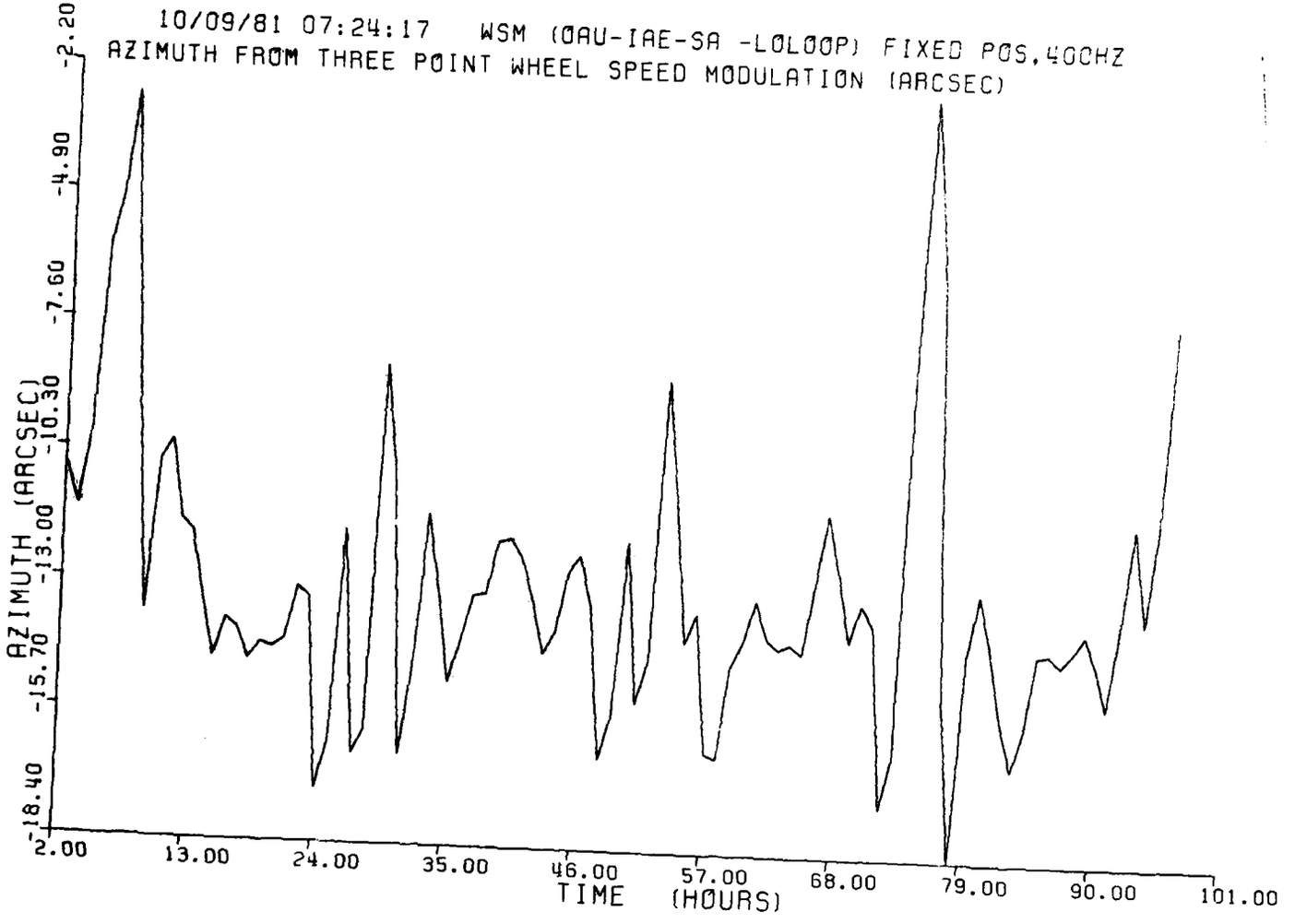

Figure 20. Uncompensated Azimuth from Torque in Figure 19.

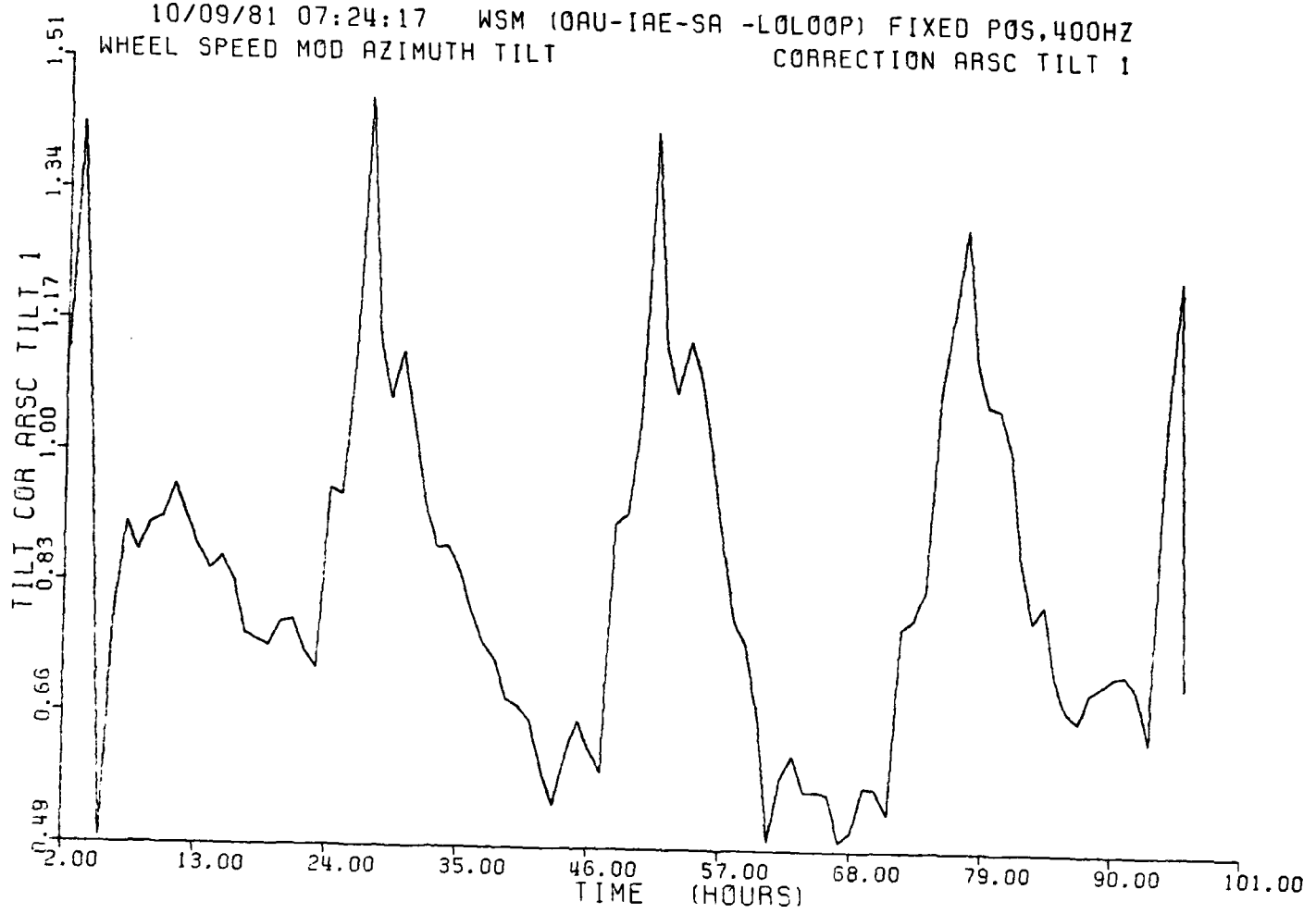

Figure 21. Tilt Compensations for Azimuth Data in Figure 20.

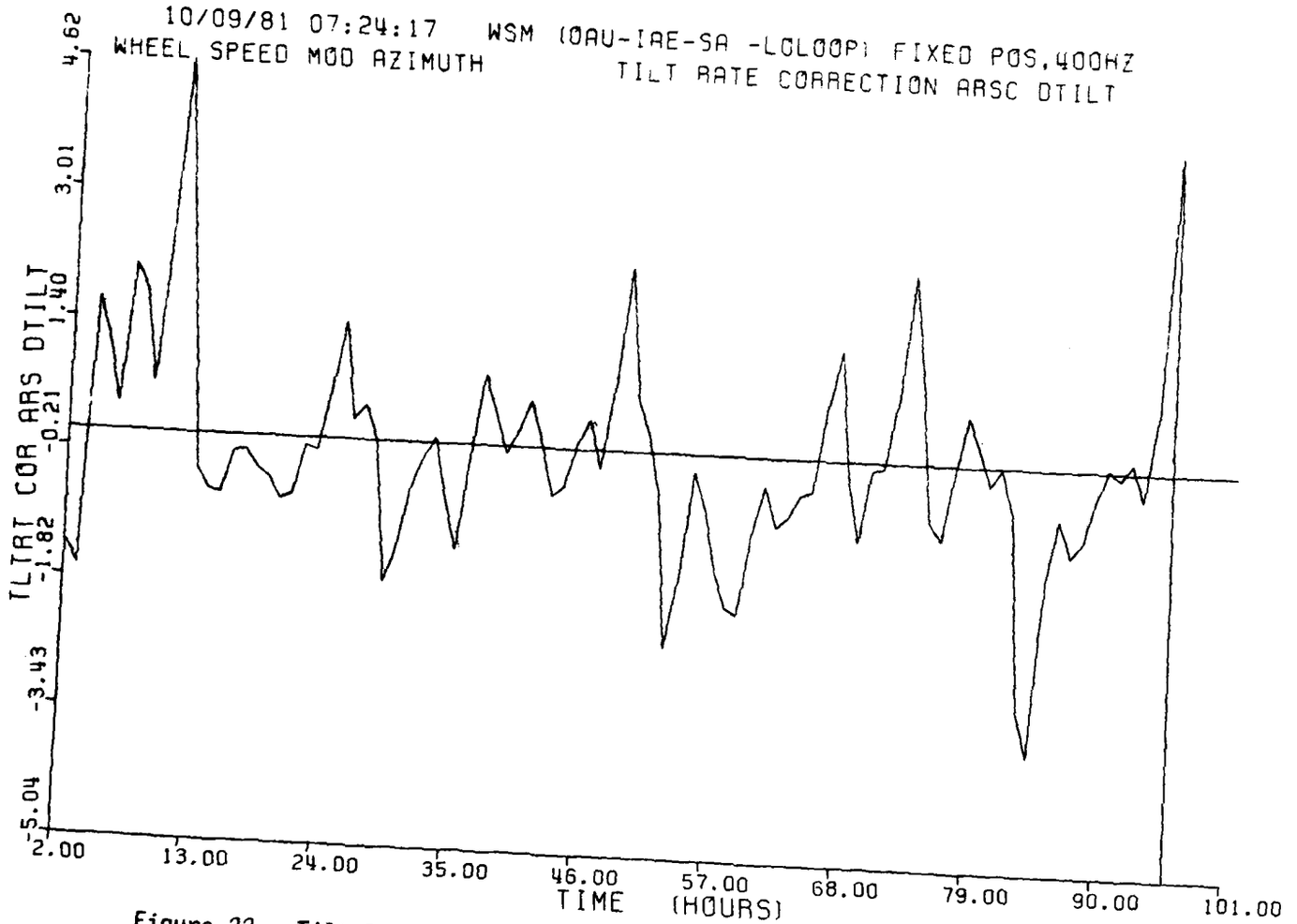

Figure 22. Tilt Rate Compensations for Azimuth Data in Figure 20.

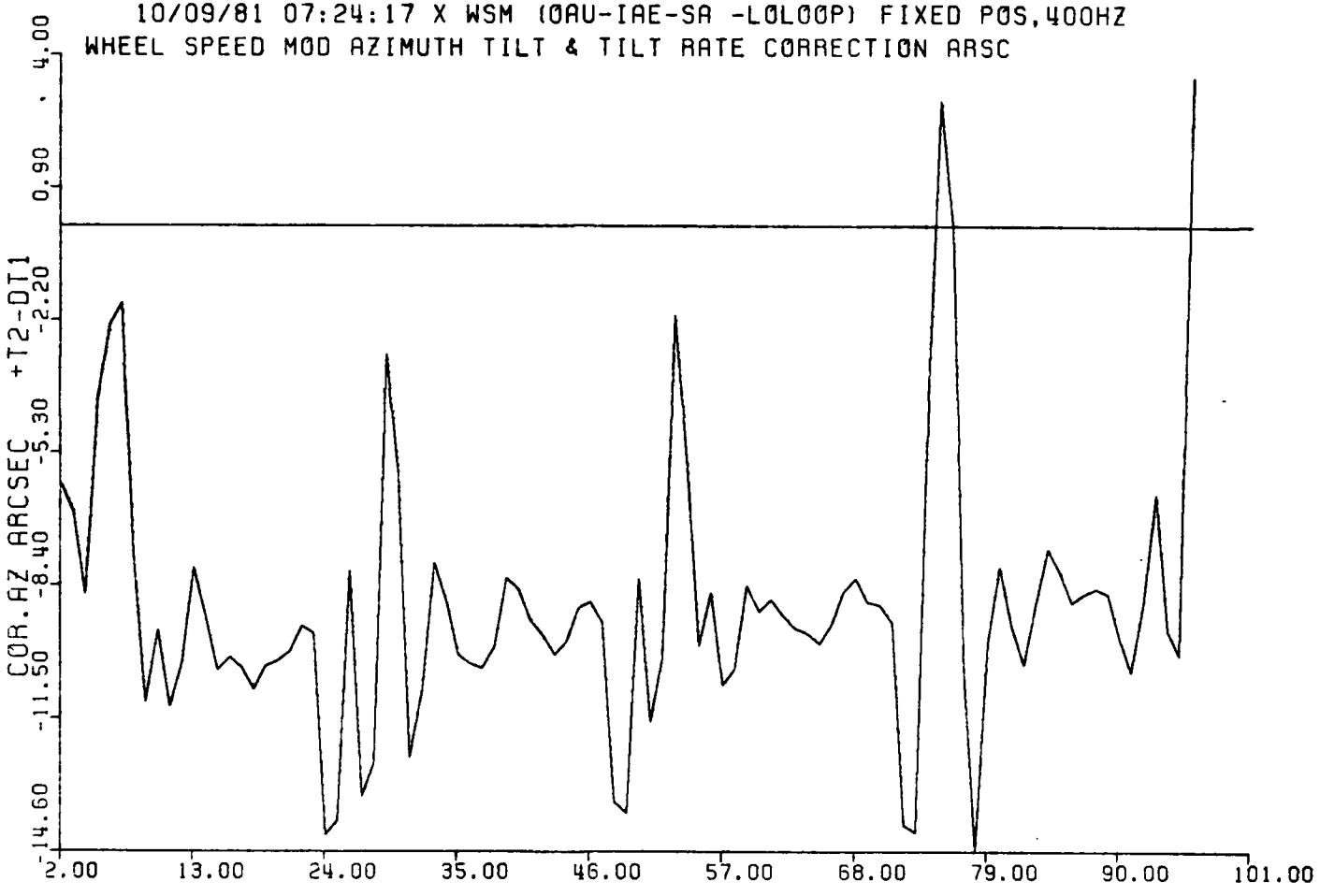

Figure 23. Compensated Azimuth for 4-Day Interval with Significant Environmental Influence.

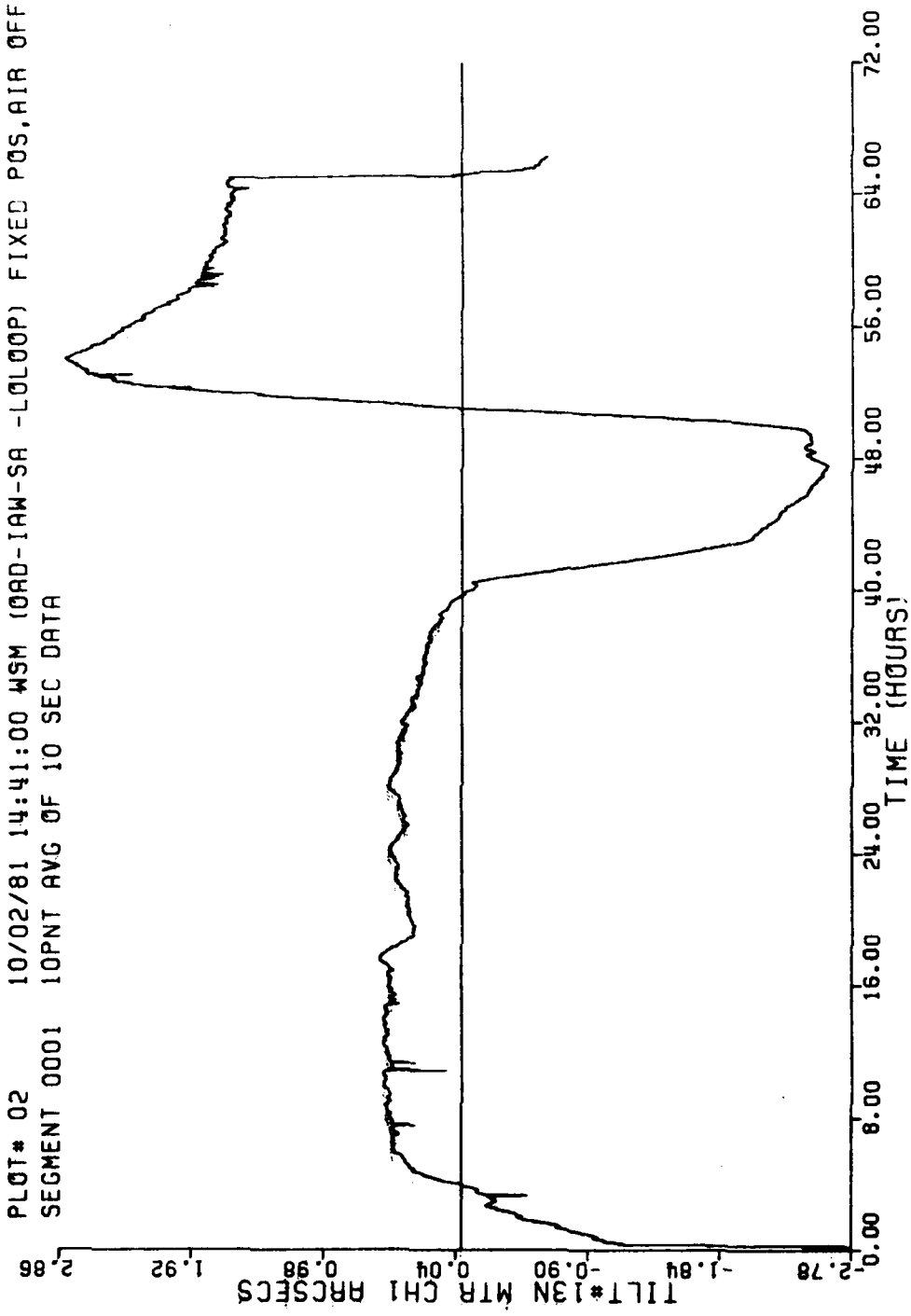

Figure 24. North Tilt During Tilt Event.

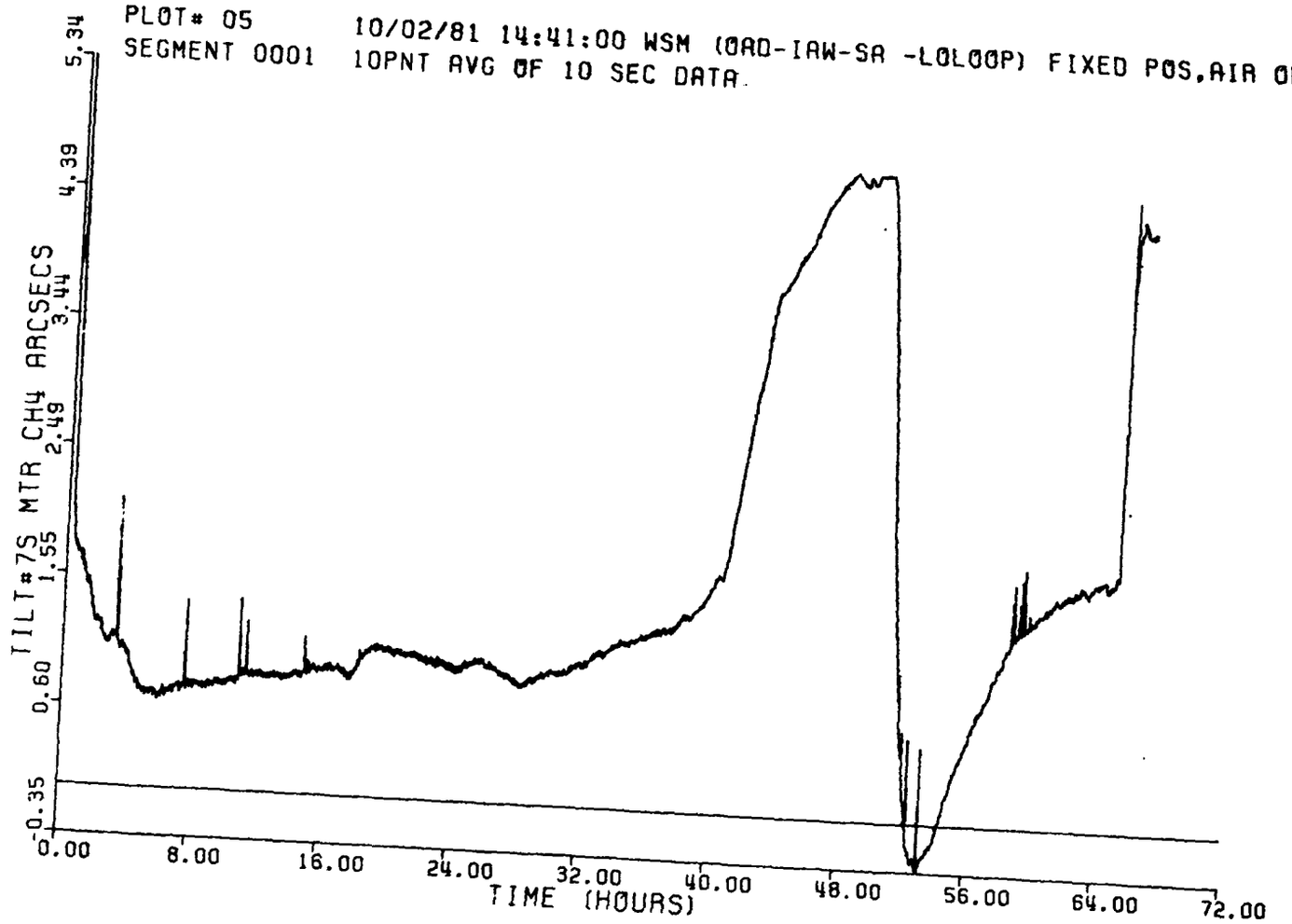

Figure 25. South Tilt During Tilt Event.

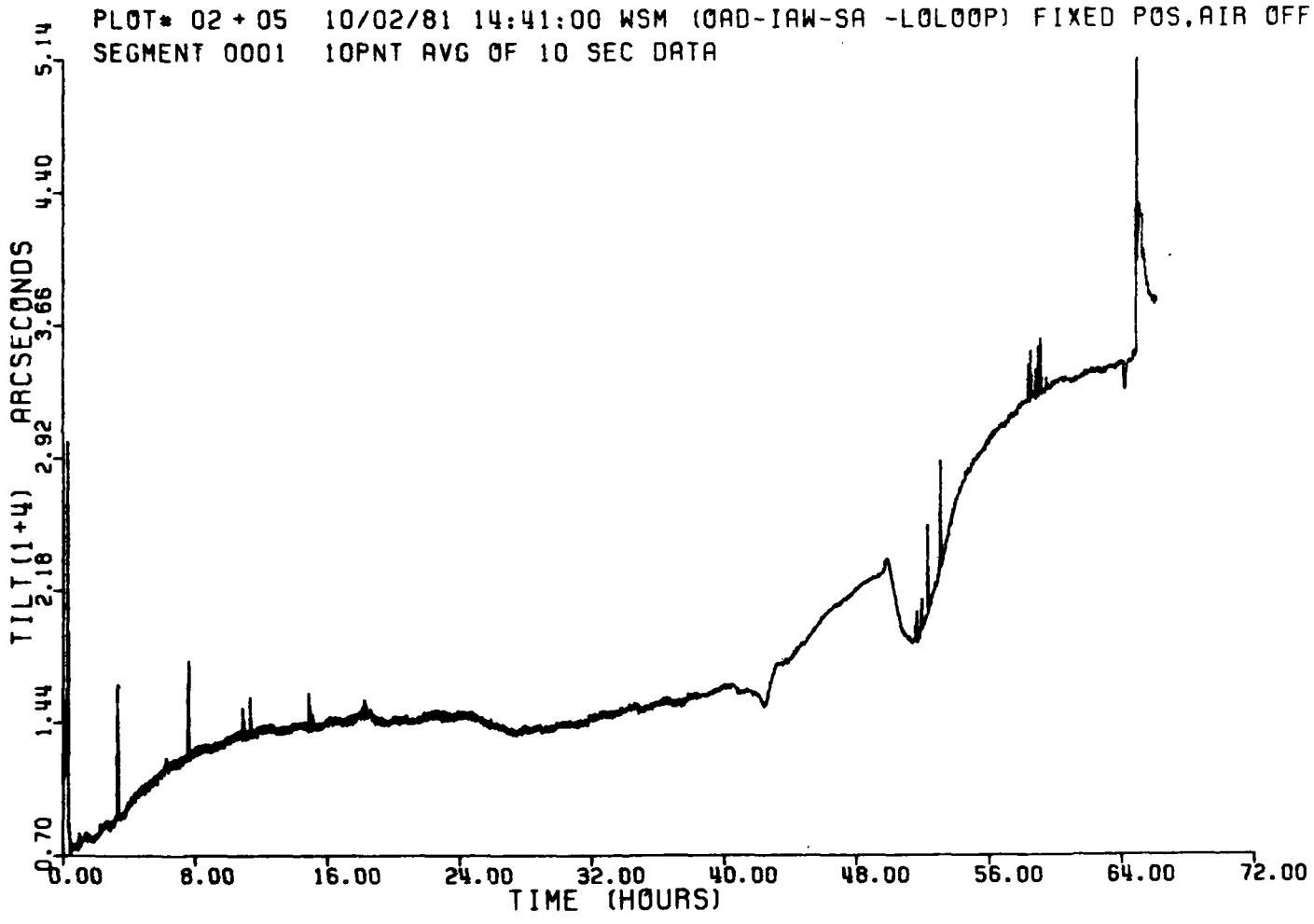

Figure 26. Sum of Anti-parallel N-S Tilt Signals.

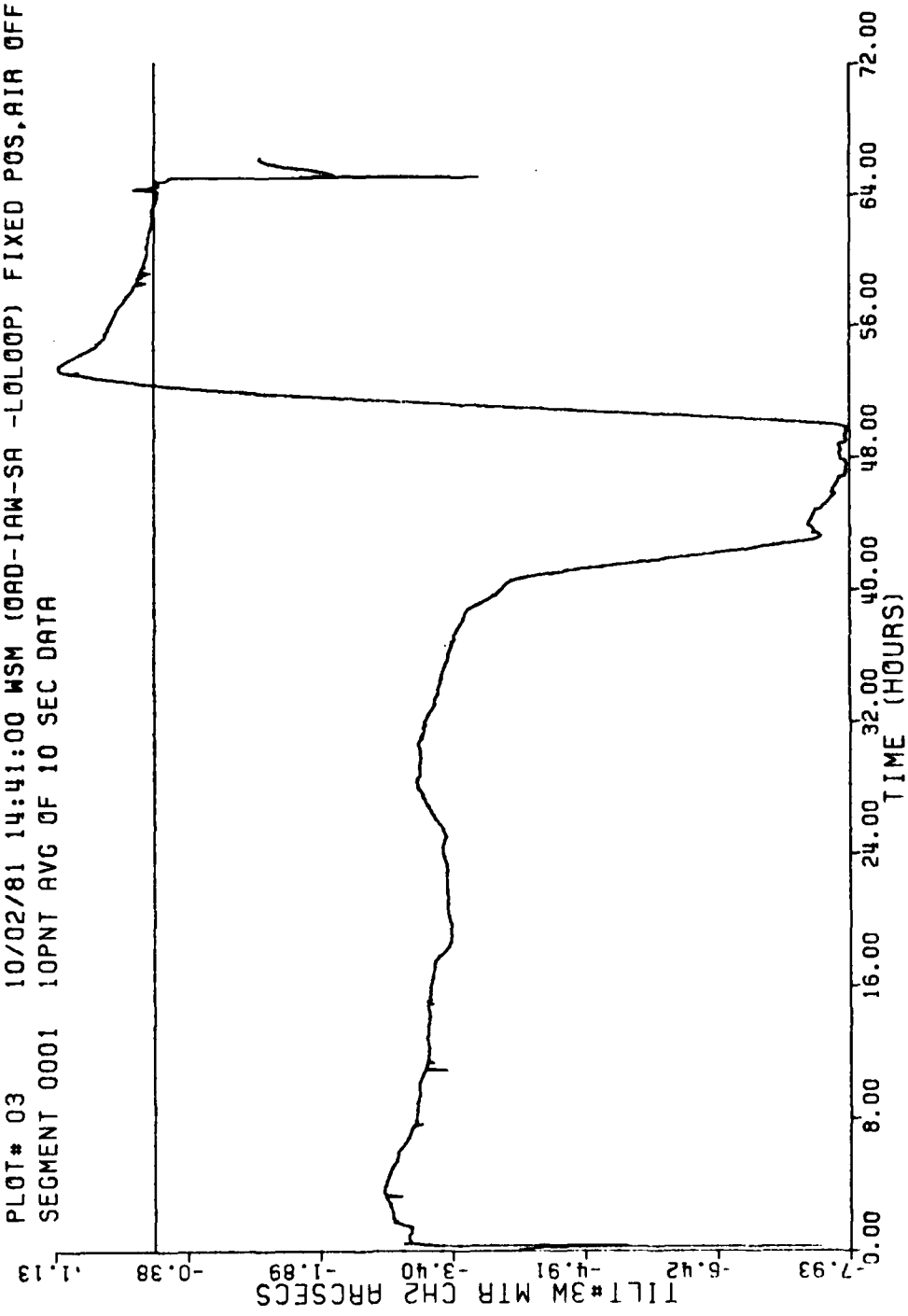

Figure 27. West Tilt During Tilt Event.

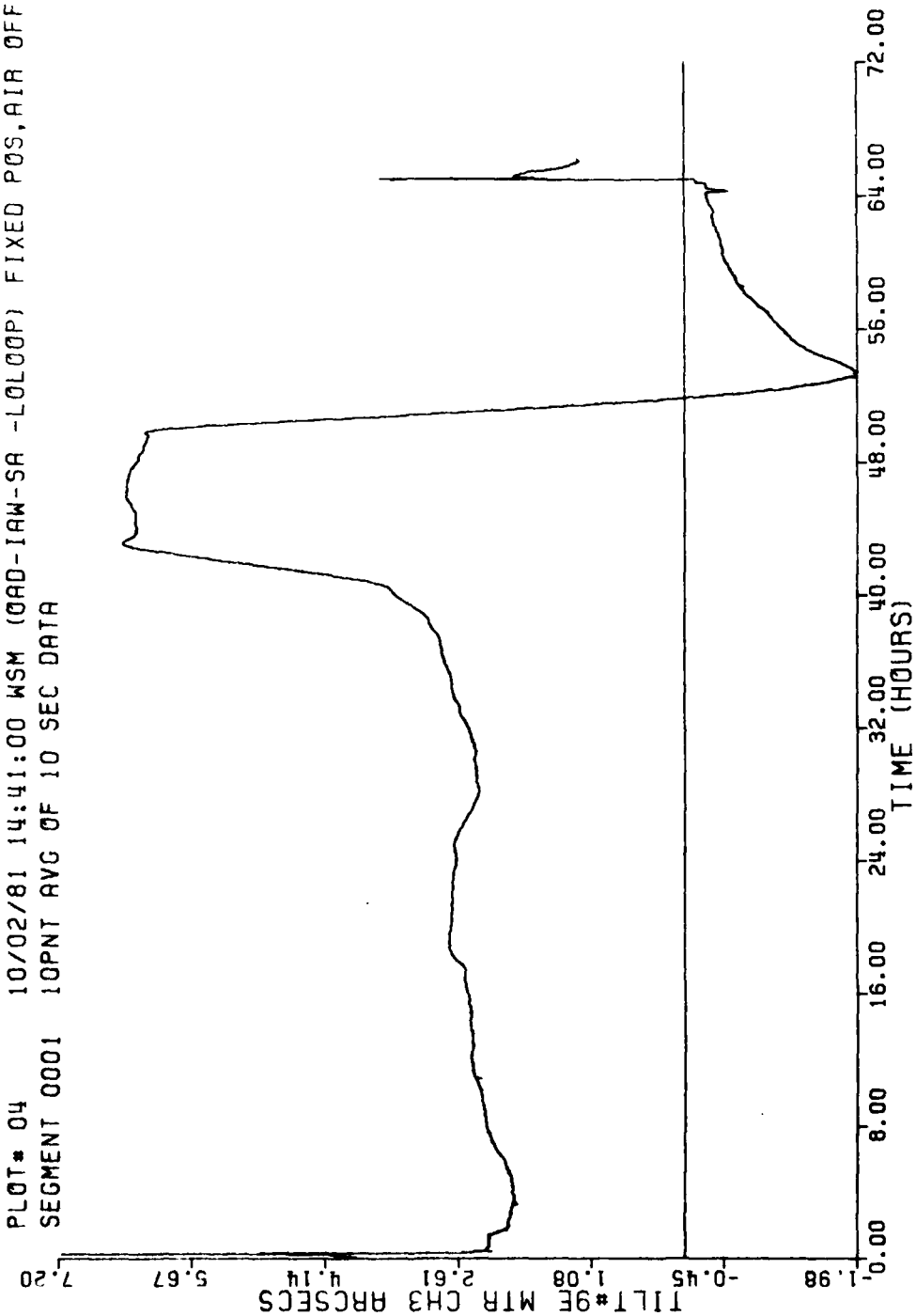

Figure 28. East Tilt During Tilt Event.

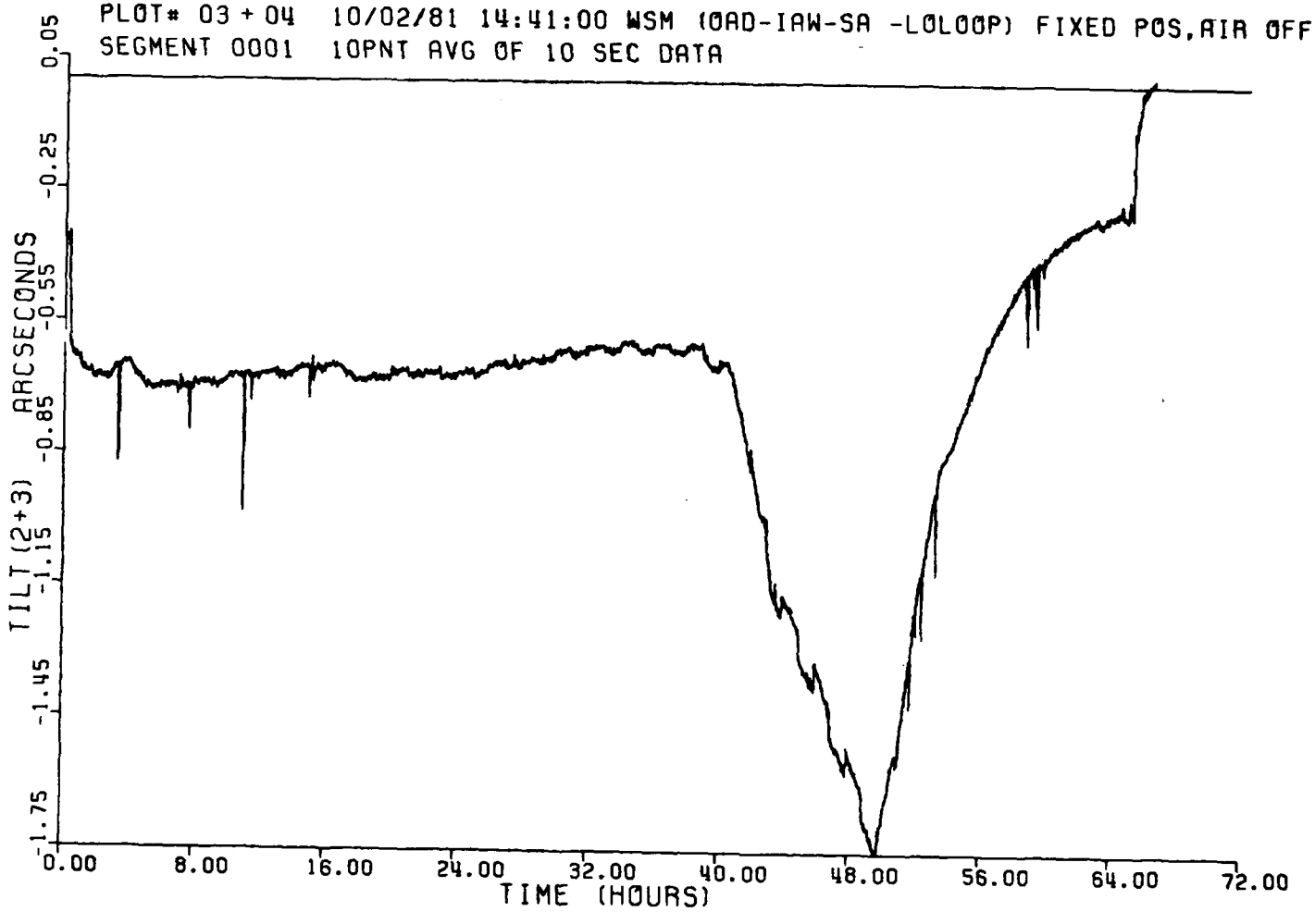

Figure 29. Sum of Anti-Parallel E-W Tilt Signals.

tilt event is the motion of the air bearing table when the air supply is turned off and then on at roughly 43 and 50 hours. The variance in measured tilt from the antiparallel pairs is readily apparent in Figures 26 and 29.

Table 1 is a comparison of the relative azimuth errors which would arise from tilt (T) and tilt rate (DT) for three test intervals. Tiltmeters T1 and T4 were antiparallel, measuring tilt about an east-west axis, and are thus used to compensate for tilt rate errors. Tiltmeters T2 and T3 were antiparallel, measuring tilt about a north-south axis, and are thus used to compensate for tilt errors. Note the difference in RMS uncertainty and range between the like tiltmeters.

Obviously, these variations make accurate compensation for tilt and tilt rate errors during azimuth measurement periods impossible, and could therefore account for at least some of the anomalous azimuthal motions frequently observed during periods of increased environmental variations.

The tiltmeters were returned to AFGL during the test program for recalibration of their respective scale factors. The new calibrations agreed with the previous calibrations to better than 3% for all four tiltmeters. Yet, when the tiltmeters were re-installed on the test station, they again disagreed significantly with each other.

This disagreement between tiltmeters could be caused by different response characteristics to high frequency accelerations or by different temperature sensitivities. Warping of the test table is also a possibility, but is not considered likely.

Temperature sensitivity of the test instrumentation is considered to be the prime candidate for explanation of the azimuth anomalies, since variations in most test parameters are correlated with changes in the ambient temperature. This is easily seen in Figures 30 and 31, which are plots of the ambient temperature in the test station enclosure and of the test laboratory wall temperature, respectively. Comparison of these plots with Figures 19-23 readily shows the correlation of temperature with the tilt, torque and apparent azimuth variations.

TABLE 2. COMPARISON OF AZIMUTH ERROR COMPENSATION FROM ANTI-PARALLEL TILTMETERS

(arc seconds of Azimuth Compensation)

Orientation 10/02/81	TILTMETER T1 -E/W	T2 +N/S	T3 -N/S	T4 +E/W	DT1	DT2	DT3	DT4	Azimuth
MEAN	-0.3	2.8	-2.2	-1.4	0.0	0.0	0.0	-0.1	-62.3
RMS	1.15	2.09	1.88	1.09	2.17	3.79	3.40	2.30	7.01
MIN	-2.6	-1.5	-6.2	-4.8	-11.9	-2.2	-9.9	-6.2	-91.2
MAX	2.7	7.9	2.3	0.4	6.4	1.1	19.2	11.7	-39.6
RANGE	5.3	9.4	8.5	5.2	18.3	3.3	29.1	17.9	51.6
10/09/81									
MEAN	0.8	4.0	-7.5	-4.8	-0.1	0.1	-0.1	-0.3	-47.5
RMS	0.22	0.51	0.14	0.29	1.33	1.11	0.41	2.41	1.99
MIN	2.7	-2.8	5.8	4.6	-2.1	-5.5	-2.0	-1.3	-52.2
MAX	3.6	-2.0	6.6	5.9	2.0	1.6	1.7	2.0	-44.1
RANGE	0.9	0.8	0.8	1.3	4.1	7.1	3.7	3.3	8.1
10/14/81									
MEAN	3.1	-2.4	6.2	5.4	0.1	0.0	0.1	0.2	-13.0
RMS	0.28	0.26	0.28	0.39	1.01	0.47	0.83	0.80	2.9
MIN	-0.5	2.9	-7.5	-5.0	-4.1	-2.3	-15.8	-22.8	-18.4
MAX	1.5	5.6	-6.9	4.6	3.8	-0.6	7.0	-5.9	-2.5
RANGE	2.0	2.7	0.6	9.6	7.9	1.7	22.8	16.9	15.9

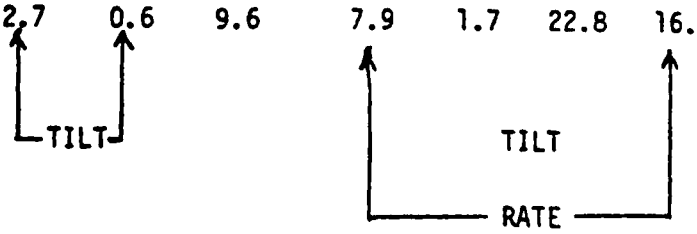

COLUMNS TO BE COMPARED FOR
RESPECTIVE COMPENSATION CONTRIBUTION

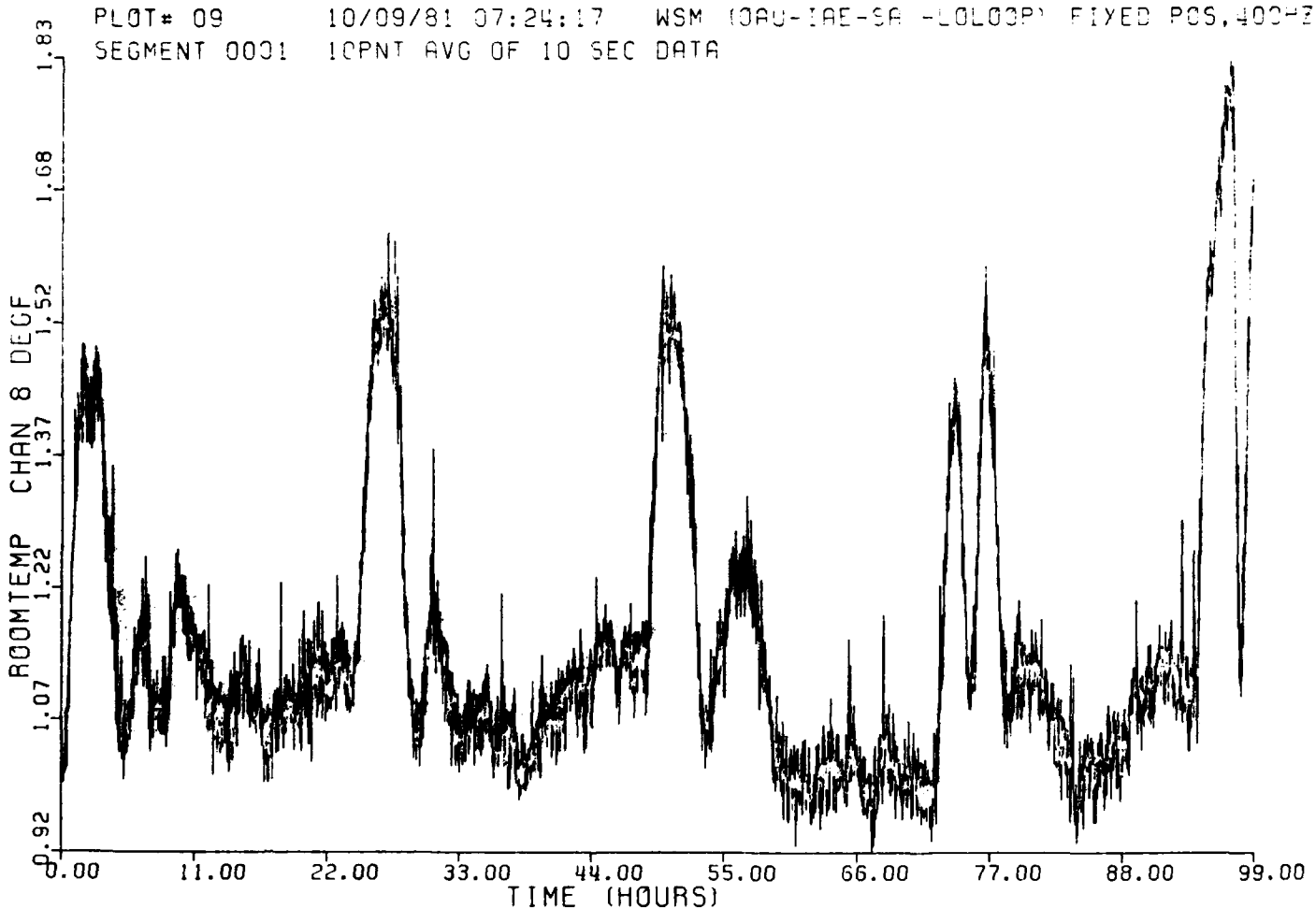

Figure 30. Test Station Ambient Temperature.

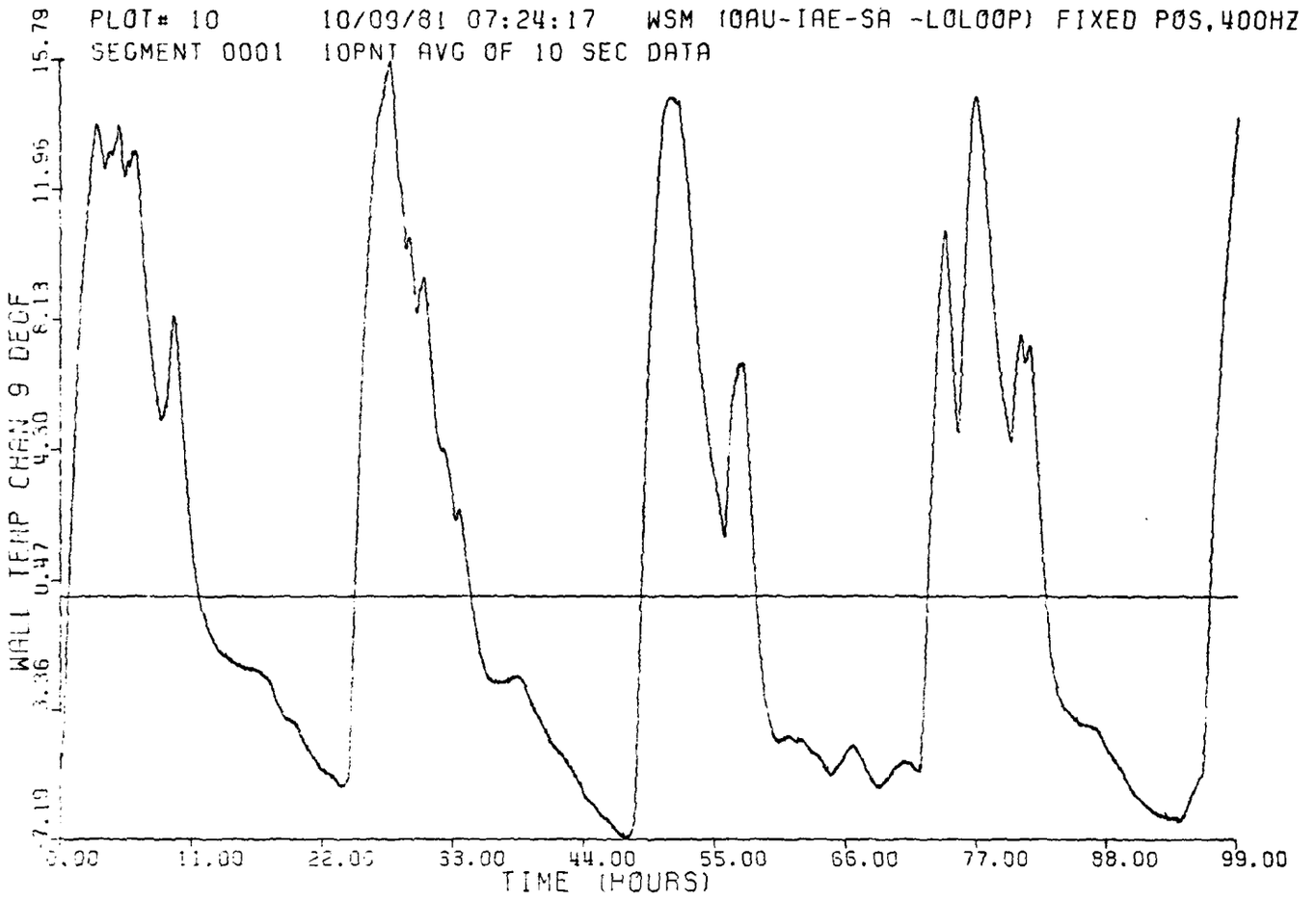

Figure 31. Test Laboratory Wall Temperature.

Finally, the higher frequency ambient motion environment was far from ideal throughout most of the test period. There was a great deal of construction activity during daylight hours which transmitted motions through the ground to the test station. The motions were the result of pile drivers and graders which operated as close at 100 feet from the test station, and were typically at frequencies around 30-50 Hz. Railroad trains, which often passed by the laboratory as frequently as 3-5 times per day, also caused large horizontal accelerations of the test station. A train detector signal was added to the data acquisition signal array to allow for removal of train-induced errors. But the detector was soon damaged by the construction and became inoperative.

In summary, the environment had a substantial impact on the test program. At this time it is difficult to separate the effects of the environment on the azimuth measuring instrumentation from the actual azimuthal motions which were induced by variations in the environment. One fact is clear, however: when designing an azimuth measuring system with a sub-arc second accuracy goal, one must be keenly aware of the effects of the environment, regardless of the technique used to measure azimuth.

5. RECOMMENDATIONS

The results of this study confirm that it is feasible to measure true azimuth to sub-arc second accuracy with WSM. This capability far surpasses the demonstrated accuracy of any known azimuth measurement technique, and is available immediately. Since the present accuracy requirements already exceed any fielded azimuth measurement capability, we highly recommend that this technology be developed into a complete system as soon as possible.

New versions of the PM gyro should be incorporated in a future azimuth measuring system. CSDL has already developed a Fourth Generation Technology Demonstration Gyroscope which has a number of

design features that would enhance the stability and repeatability of WSM azimuth measurement. However, even this gyro was designed as an inertial navigation gyro which can withstand large acceleration inputs. Since this condition is not required for azimuth measurement, optimization of the design should be considered for this specific application.

Lasers should be used for azimuth transfer to the test article. CSDL is presently evaluating laser technology as part of its on-going independent research and development programs. These evaluations indicate that lasers could be incorporated with PM gyros to complete an azimuth measuring system that could achieve sub-arc second accuracy at the system level.

Finally, the one lingering uncertainty associated with this feasibility study -- the anomalous behavior of the gyro which was correlated with a varying environment -- should be studied further. In any event, this condition could probably be minimized by operating a future azimuth measuring system on a tilt isolation table in a thermally - controlled enclosure. This requirement is not unrealistic since the ultimate accuracies are desired in test laboratories where these conditions can be reasonably well controlled.

ACKNOWLEDGEMENTS

The contributions from the following Engineers and Technicians are greatly appreciated. The success of this investigation is directly attributable to the individual and combined efforts of each of these people and many others who provide daily support to them.

Mr. Michael Ash	Software Development
Ms. Nancy DiMento	Data Processing
Mr. Richard DiPaola	Program Direction
Ms. Julia Hekimian	Report Typing
Mr. John Hengeveld	Computer Hardware and Software Development
Mr. Marco Marchi	Electrical Engineering
Mr. Gerard McWeeney	Electrical Engineering
Mr. Joseph Miola	Test and Analysis Consultation
Mr. George Nutting	Test Technician
Mr. William Oulighan	Test and Analysis Consultation
Mr. Joseph Scoppettuolo	Electrical Engineering
Mr. Paul Steranka	Test Preparation and Analysis
Mr. James Shearer	Program Manager

APPENDIX A

EFFECTS OF INSTRUMENT MISALIGNMENTS ON WSM AZIMUTH DETERMINATIONS

1. SUMMARY

Model equations are presented for comparing traditional 4-position gyrocompass and wheel-speed-modulation azimuth estimates. Simulated data was used to check out the model equations. Application of these equations to PM-1 data indicates that there is a systematic unmodelled error source causing relatively poor agreement between the two methods. Table tilt was investigated as a possible cause, but did not account for the systematic error.

2. TORQUE EQUATIONS AT FULL AND HALF WHEEL SPEED

The model equations in torque at full and half wheel speed (full and half angular momentum) with OA vertical are given in Figure 1.

3. MODEL EQUATIONS FOR 4-POSITION GYROCOMPASSING

The model equations in torque for 4-position gyrocompassing with OA vertical at full and half wheel speed are given in Figures 2 and 3. The traditional estimation equations are given in Figures 4 and 5. The effects of tilt and tilt rate have been neglected. Note that, on a torque basis, the equation for the azimuth estimate is different at full and half wheel speed. Also note that an estimate for IA misalignment about SA is available from the combined full and half-H data.

4. AZIMUTH ESTIMATION WITH WHEEL SPEED MODULATION

The equations for azimuth estimation from wheel-speed-modulation data are given in Figures 6 and 7.

5. SIMULATION STUDY

Simulated data is listed in Figure 8. The traditional 4-position gyrocompassing estimates are given in Figure 9, along with azimuth estimates from wheel speed modulation using various degrees of compensation. Note that the correct azimuth estimates from wheel speed modulation are

not recovered until compensation for delta bias and IA misalignments about OA and SA are included.

6. ANALYSIS OF PM-1 DATA

Analysis of data from gyro PM-1 gyrocompassing at full and half wheel speed is given in Figure 10. The traditional 4-position gyrocompass analysis yields significantly different estimates for azimuth, as well as for IA misalignment about OA, both of which are unexplainable, as yet. Table tilt was evaluated and found not to be the cause. The wheel-speed-modulation analysis yields clustering of azimuth estimates from OA-up and OA-down. The fact that both OA-up estimates are similar and both OA-down estimates are similar gives confidence that the clustering will be explainable by systematic unmodelled errors.

The differences between the traditional 4-position gyrocompassing and wheel-speed-modulation azimuth estimates can be attributed quantitatively to the apparent differences in IA misalignment about OA and azimuth between full and half wheel speed. This is illustrated in Figure 11. However, the apparent changes in IA misalignment about OA and azimuth with wheel speed are still anomalous at this time. The compatibility between the wheel-speed-modulation and traditional 4-position gyrocompassing azimuth estimates is strictly a mathematical artifice to demonstrate compatibility between the two methods of analysis.

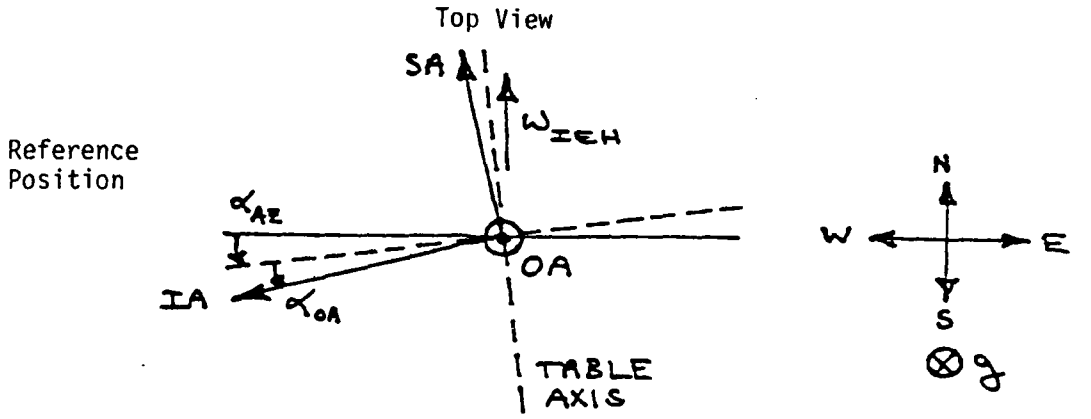

α_{AZ} = Misalignment of Table Reference in azimuth (RAD)

α_{OA} = IA misalignment about OA from table reference (RAD)

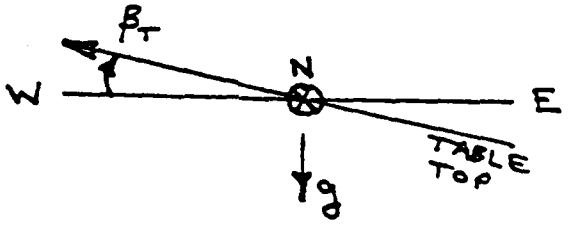

β_T = Tilt of table top about north-south axis (RAD)

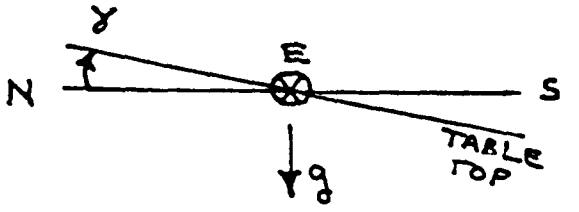

γ = Tilt of table top about east-west axis (RAD)

Figure 1a. Definition of Angles

$$M_F = H\omega_{IEH} (\pm \alpha_{AZ} \pm \alpha_{OA}) + H\omega_{IEV} (\pm \beta_{SA} \pm \beta_{TF}) \pm H\omega_{\gamma F}$$

$$+ (D_F)_T + (D_0)_T g_{OA} + (D_{00})_T g_{OA}^2$$

$$M_H = \frac{1}{2} H\omega_{IEH} (\pm \alpha_{AZ} \pm \alpha_{OA}) + \frac{1}{2} H\omega_{IEV} (\pm \beta_{SA} \pm \beta_{TH}) \pm \frac{1}{2} H\omega_{\gamma H}$$

$$+ (D_F)_T + (\Delta D_F)_T + (D_0)_T g_{OA} + (D_{00})_T g_{OA}^2$$

$$M_F' = \omega_{IEH}' (\pm \alpha_{AZ} \pm \alpha_{OA}) + \omega_{IEV}' (\pm \beta_{SA} \pm \beta_{TF}) \pm \omega_{\gamma F}'$$

$$+ D_F + D_0 g_{OA} + D_{00} g_{OA}^2$$

$$M_H' = \frac{1}{2} \omega_{IEH}' (\pm \alpha_{AZ} \pm \alpha_{OA}) + \frac{1}{2} \omega_{IEV}' (\pm \beta_{SA} \pm \beta_{TH}) \pm \frac{1}{2} \omega_{\gamma H}'$$

$$+ D_F + \Delta D_F + D_0 g_{OA} + D_{00} g_{OA}^2$$

Note: Small-angle approximations have been used.

where:

$$M_{F,H}' = M_{F,H} \left(\frac{10^3}{H\omega_{IE}}\right) \quad \text{Full-H Meru}$$

$$\omega_{IEH,IEV}' = \omega_{IEH,IEV}' \left(\frac{10^3}{\omega_{IE}}\right) \quad \text{Meru}$$

$$\omega_{\gamma F,\gamma H}' = \omega_{\gamma F,\gamma H} \left(\frac{10^3}{\omega_{IE}}\right) \quad \text{Meru}$$

$$D_i = (D_i)_T \left(\frac{10^3}{H\omega_{IE}}\right) \text{ Full-H Meru}$$

$M_{F,H}$ = Torque at full, half wheel speed (dyne-cm)

H = Wheel angular momentum (dyne-cm-sec)

ω_{IE} = Earth rate (rad/sec)

$\omega_{IEH}, \omega_{iEV}$ = Horizontal, vertical components of earth rate (rad/sec)

β_{SA} = IA misalignment about SA from table top (RAD)

$\omega_{\gamma F}, \omega_{\gamma H}$ = Tilt rate about east-west axis during full, half wheel speed torque measurements (rad/sec)

$(D_F)_T, (D_0)_T, (D_{00})_T$ = Gyro error coefficients (dyne-cm, dyne-cm/g, dyne-cm/g^2)

$(\Delta D_F)_T$ = Change in D_F from full to half wheel speed (dyne-cm)

Figure 1b. Torque Equations at Full and Half Wheel Speed with OA Vertical

Position 1
OA-Up, IA-West

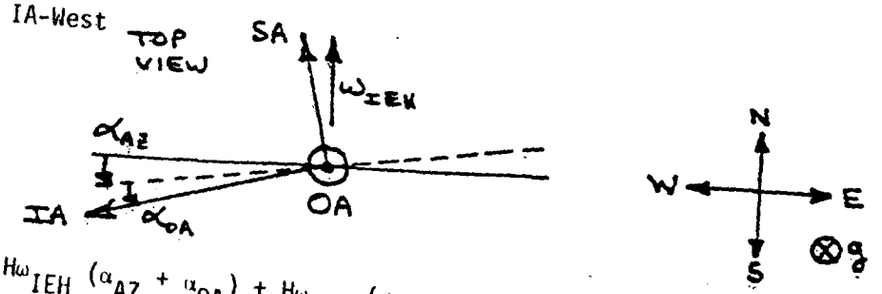

$$M_{1F} = - H\omega_{IEH} (\alpha_{AZ} + \alpha_{OA}) + H\omega_{IEV} (\beta_{SA} + \beta_{1TF}) - H\omega_{1\gamma F} + (D_F)_T - (D_0)_T + (D_{00})_T$$

$$M_{1H} = - \frac{1}{2} H\omega_{IEH} (\alpha_{AZ} + \alpha_{OA}) + \frac{1}{2} H\omega_{IEV} (\beta_{SA} + \beta_{1TH}) - \frac{1}{2} H\omega_{1\gamma H} + (D_F)_T - (D_0)_T + (D_{00})_T + (\Delta D_F)_T$$

Position 2
OA-Up, IA-East

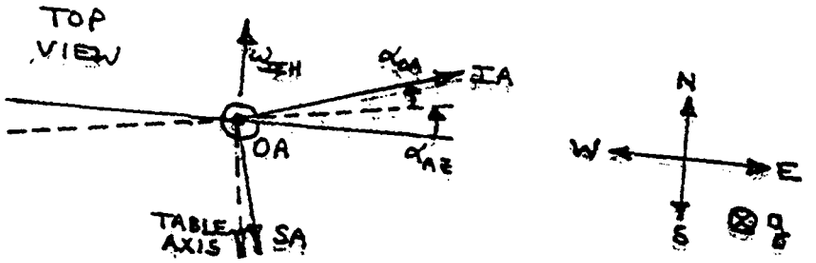

$$M_{2F} = H\omega_{IEH} (\alpha_{AZ} + \alpha_{OA}) + H\omega_{IEV} (\beta_{SA} - \beta_{2TF}) + H\omega_{2\gamma F} + (D_F)_T - (D_0)_T + (D_{00})_T$$

$$M_{2H} = \frac{1}{2} H\omega_{IEH} (\alpha_{AZ} + \alpha_{OA}) + \frac{1}{2} H\omega_{IEV} (\beta_{SA} - \beta_{2TH}) + \frac{1}{2} H\omega_{2\gamma H} + (D_F)_T - (D_0)_T + (D_{00})_T + (\Delta D_F)_T$$

Position 3
OA-Down, IA-West

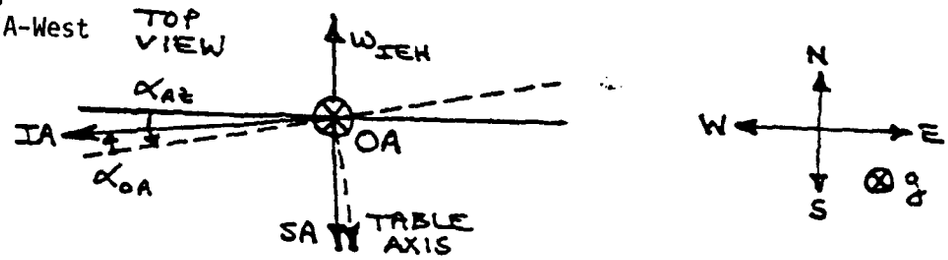

$$M_{3F} = - H\omega_{IEH} (\alpha_{AZ} - \alpha_{OA}) - H\omega_{IEV} (\beta_{SA} - \beta_{3TF}) - H\omega_{3\gamma F} + (D_F)_T + (D_0)_T + (D_{00})_T$$

$$M_{3H} = - \frac{1}{2} H\omega_{IEH} (\alpha_{AZ} - \alpha_{OA}) - \frac{1}{2} H\omega_{IEV} (\beta_{SA} - \beta_{3TH}) - \frac{1}{2} H\omega_{3\gamma H} + (D_F)_T + (D_0)_T + (D_{00})_T + (\Delta D_F)_T$$

Position 4
OA-Down, IA-East

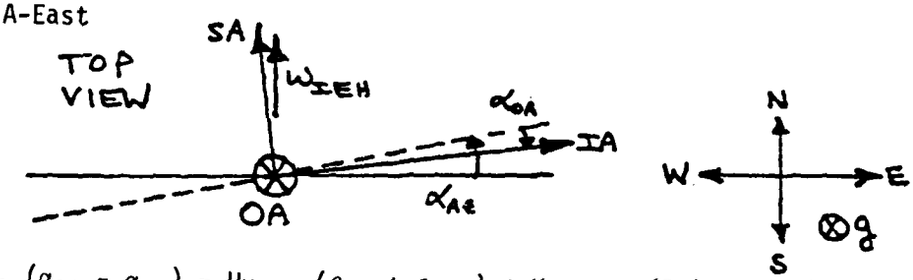

$$M_{4F} = H\omega_{IEA} (\alpha_{AZ} - \alpha_{OA}) - H\omega_{IEV} (\beta_{SA} + \beta_{4TF}) + H\omega_{4\gamma F} + (D_F)_T + (D_0)_T + (D_{00})_T$$

$$M_{4H} = \frac{1}{2} H\omega_{IEH} (\alpha_{AZ} - \alpha_{OA}) - \frac{1}{2} H\omega_{IEV} (\beta_{SA} + \beta_{4TH}) + \frac{1}{2} H\omega_{4\gamma H} + (D_F)_T + (D_0)_T + (D_{00})_T + (\Delta D_F)_T$$

Figure 2. Four-Position Gyrocompassing Torque Equations in Dyne-CM

Position 1: OA-Up, IA-West

$$M'_{1F} = -\omega'_{IEH}(\alpha_{AZ} + \alpha_{OA}) + \omega'_{IEV}(\beta_{SA} + \beta_{1TF}) - \omega'_{1\gamma F} + D_F - D_0 + D_{00}$$

$$M'_{1H} = -\frac{1}{2}\omega'_{IEH}(\alpha_{AZ} + \alpha_{OA}) + \frac{1}{2}\omega'_{IEV}(\beta_{SA} + \beta_{1TH}) - \frac{1}{2}\omega'_{1\gamma H} + D_F - D_0 + D_{00} + \Delta D_F$$

Position 2: OA-Up, IA-East

$$M'_{2F} = \omega'_{IEH}(\alpha_{AZ} + \alpha_{OA}) + \omega'_{IEV}(\beta_{SA} - \beta_{2TF}) + \omega'_{2\gamma F} + D_F - D_0 + D_{00}$$

$$M'_{2H} = \frac{1}{2}\omega'_{IEH}(\alpha_{AZ} + \alpha_{OA}) + \frac{1}{2}\omega'_{IEV}(\beta_{SA} - \beta_{2TH}) + \frac{1}{2}\omega'_{2\gamma H} + D_F - D_0 + D_{00} + \Delta D_F$$

Position 3: OA-Down, IA-West

$$M'_{3F} = -\omega'_{IEH}(\alpha_{AZ} - \alpha_{OA}) - \omega'_{IEV}(\beta_{SA} - \beta_{3TF}) - \omega'_{3\gamma F} + D_F + D_0 + D_{00}$$

$$M'_{3H} = -\frac{1}{2}\omega'_{IEH}(\alpha_{AZ} - \alpha_{OA}) - \frac{1}{2}\omega'_{IEV}(\beta_{SA} - \beta_{3TH}) - \frac{1}{2}\omega'_{3\gamma H} + D_F + D_0 + D_{00} + \Delta D_F$$

Position 4: OA-Down, IA-East

$$M'_{4F} = \omega'_{IEH}(\alpha_{AZ} - \alpha_{OA}) - \omega'_{IEV}(\beta_{SA} + \beta_{4TF}) + \omega'_{4\gamma F} + D_F + D_0 + D_{00}$$

$$M'_{4H} = \frac{1}{2}\omega'_{IEH}(\alpha_{AZ} - \alpha_{OA}) - \frac{1}{2}\omega'_{IEV}(\beta_{SA} + \beta_{4TH}) + \frac{1}{2}\omega'_{4\gamma H} + D_F + D_0 + D_{00} + \Delta D_F$$

Figure 3. Four-Position Gyrocompassing Torque Equations in Full-H Meru

Full Wheel Speed:

$$\alpha_{AZ} = \frac{(M_{2F} + M_{4F} - M_{1F} - M_{3F})}{4H\omega_{IEH}} \text{ Rad}$$

$$\alpha_{OA} = \frac{(M_{2F} + M_{3F} - M_{1F} - M_{4F})}{4H\omega_{IEH}} \text{ Rad}$$

$$\beta_{SA} - \frac{(D_0)_T}{H\omega_{IEV}} = \frac{(M_{1F} + M_{2F} - M_{3F} - M_{4F})}{4H\omega_{IEV}} \quad \text{Rad (Equivalent)}$$

$$(D_F)_T + (D_{00})_T = \frac{1}{4}(M_{1F} + M_{2F} + M_{3F} + M_{4F}) \text{ Dyne-cm}$$

Half Wheel Speed:

$$\alpha_{AZ} = \frac{(M_{2H} + M_{4H} - M_{1H} - M_{3H})}{2H\omega_{IEH}} \text{ Rad}$$

$$\alpha_{OA} = \frac{(M_{2H} + M_{3H} - M_{1H} - M_{4H})}{2H\omega_{IEH}} \text{ Rad}$$

$$\beta_{SA} - \frac{2(D_0)_T}{H\omega_{IEV}} = \frac{(M_{1H} + M_{2H} - M_{3H} - M_{4H})}{2H\omega_{IEV}} \quad \text{Rad (Equivalent)}$$

$$(D_F)_T + (D_{00})_T + (\Delta D_F)_T = \frac{1}{4}(M_{1H} + M_{2H} + M_{3H} + M_{4H}) \text{ Dyne-cm}$$

β_{SA} and $(\Delta D_F)_T$ Estimates:

$$\beta_{SA} = \frac{[(M_{1F} + M_{2F} - M_{3F} - M_{4F}) - (M_{1H} + M_{2H} - M_{3H} - M_{4H})]}{2H\omega_{IEV}} \text{ Rad}$$

$$(\Delta D_F)_T = \frac{[(M_{1H} + M_{2H} + M_{3H} + M_{4H}) - (M_{1F} + M_{2F} + M_{3F} + M_{4F})]}{4} \text{ Dyne-cm}$$

Note: β_T and ω_γ have been assumed negligible.

Figure 4. Traditional Four-Position Gyrocompass Estimates Using Torque Output in Dyne-cm.

Full Wheel Speed:

$$\alpha_{AZ} = \frac{(M'_{2F} + M'_{4F} - M'_{1F} - M'_{3F})}{4\omega'_{IEH}} \text{ Rad}$$

$$\alpha_{OA} = \frac{(M'_{2F} + M'_{3F} - M'_{1F} - M'_{4F})}{4\omega'_{IEH}} \text{ Rad}$$

$$\beta_{SA} - \frac{D_O}{\omega'_{IEV}} = \frac{(M'_{1F} + M'_{2F} - M'_{3F} - M'_{4F})}{4\omega'_{IEV}} \quad \text{Rad (Equivalent)}$$

$$D_F + D_{OO} = \frac{1}{4}(M'_{1F} + M'_{2F} + M'_{3F} + M'_{4F}) \quad \text{Full-H Meru}$$

Half Wheel Speed:

$$\alpha_{AZ} = \frac{(M'_{2H} + M'_{4H} - M'_{1H} - M'_{3H})}{2\omega'_{IEH}} \text{ Rad}$$

$$\alpha_{OA} = \frac{(M'_{2H} + M'_{3H} - M'_{1H} - M'_{4H})}{2\omega'_{IEH}} \text{ Rad}$$

$$\beta_{SA} - \frac{2D_O}{\omega'_{IEV}} = \frac{(M'_{1H} + M'_{2H} - M'_{3H} - M'_{4H})}{2\omega'_{IEV}} \quad \text{Rad (Equivalent)}$$

$$D_F + D_{OO} + \Delta D_F = \frac{1}{4}(M'_{1H} + M'_{2H} + M'_{3H} + M'_{4H}) \quad \text{Full-H Meru}$$

β_{SA} and ΔD_F Estimates:

$$\beta_{SA} = \frac{[(M'_{1F} + M'_{2F} - M'_{3F} - M'_{4F}) - (M'_{1H} + M'_{2H} - M'_{3H} - M'_{4H})]}{2\omega'_{IEV}} \text{ Rad}$$

$$\Delta D_F = \frac{[(M'_{1H} + M'_{2H} + M'_{3H} + M'_{4H}) - (M'_{1F} + M'_{2F} + M'_{3F} + M'_{4F})]}{4} \text{ Full-H Meru}$$

Note: β_T and ω_Y have been assumed negligible.

Figure 5. Traditional Four-Position Gyrocompass Estimates Using Torque Output in Full-H Meru

OA-Up, IA-West:

$$\alpha_{AZ} = -\frac{2[M_{1F} - M_{1H} + (\Delta D_F)_T]}{H\omega_{IEH}} - \alpha_{OA} + \left(\frac{\omega_{IEV}}{\omega_{IEH}}\right)\beta_{SA}$$

$$+ \left(\frac{\omega_{IEV}}{\omega_{IEH}}\right)(2\beta_{1TF} - \beta_{1TH}) - \frac{(2\omega_{1\gamma F} - \omega_{1\gamma H})}{\omega_{IEH}}$$

OA-Up, IA-East:

$$\alpha_{AZ} = \frac{2[M_{2F} - M_{2H} + (\Delta D_F)_T]}{H\omega_{IEH}} - \alpha_{OA} - \left(\frac{\omega_{IEV}}{\omega_{IEH}}\right)\beta_{SA}$$

$$+ \left(\frac{\omega_{IEV}}{\omega_{IEH}}\right)(2\beta_{2TF} - \beta_{2TH}) - \frac{(2\omega_{2\gamma F} - \omega_{2\gamma H})}{\omega_{IEH}}$$

OA-Down, IA-West:

$$\alpha_{AZ} = -\frac{2[M_{3F} - M_{3H} + (\Delta D_F)_T]}{H\omega_{IEH}} + \alpha_{OA} - \left(\frac{\omega_{IEV}}{\omega_{IEH}}\right)\beta_{SA}$$

$$+ \left(\frac{\omega_{IEV}}{\omega_{IEH}}\right)(2\beta_{3TF} - \beta_{3TH}) - \frac{(2\omega_{3\gamma F} - \omega_{3\gamma H})}{\omega_{IEH}}$$

OA-Down, IA-East:

$$\alpha_{AZ} = \frac{2[M_{4F} - M_{4H} + (\Delta D_F)_T]}{H\omega_{IEH}} + \alpha_{OA} + \left(\frac{\omega_{IEV}}{\omega_{IEH}}\right)\beta_{SA}$$

$$+ \left(\frac{\omega_{IEV}}{\omega_{IEH}}\right)(2\beta_{4TF} - \beta_{4TH}) - \frac{(2\omega_{4\gamma F} - \omega_{4\gamma H})}{\omega_{IEH}}$$

Figure 6. Wheel-Speed-Modulation Azimuth Estimation Using Torque Output in Dyne-cm

OA-Up, IA-West:

$$\alpha_{AZ} = -\frac{2[M'_{1F} - M'_{1H} + \Delta D_F]}{\omega'_{IEH}} - \alpha_{OA} + \left(\frac{\omega'_{IEV}}{\omega'_{IEH}}\right)\beta_{SA}$$

$$+ \left(\frac{\omega'_{IEV}}{\omega'_{IEH}}\right)(2\beta_{1TF} - \beta_{1TH}) - \frac{(2\omega'_{1\gamma F} - \omega'_{1\gamma H})}{\omega'_{IEH}}$$

OA-Up, IA-East:

$$\alpha_{AZ} = \frac{2[M'_{2F} - M'_{2H} + \Delta D_F]}{\omega'_{IEH}} - \alpha_{OA} - \left(\frac{\omega'_{IEV}}{\omega'_{IEH}}\right)\beta_{SA}$$

$$+ \left(\frac{\omega'_{IEV}}{\omega'_{IEH}}\right)(2\beta_{2TF} - \beta_{2TH}) - \frac{(2\omega'_{2\gamma F} - \omega'_{2\gamma H})}{\omega'_{IEH}}$$

OA-Down, IA-West:

$$\alpha_{AZ} = -\frac{2[M'_{3F} - M'_{3H} + \Delta D_F]}{\omega'_{IEH}} + \alpha_{OA} - \left(\frac{\omega'_{IEV}}{\omega'_{IEH}}\right)\beta_{SA}$$

$$+ \left(\frac{\omega'_{IEV}}{\omega'_{IEH}}\right)(2\beta_{3TF} - \beta_{3TH}) - \frac{(2\omega'_{3\gamma F} - \omega'_{3\gamma H})}{\omega'_{IEH}}$$

OA-Down, IA-East:

$$\alpha_{AZ} = \frac{2[M'_{4F} - M'_{4H} + \Delta D_F]}{\omega'_{IEH}} + \alpha_{OA} + \left(\frac{\omega'_{IEV}}{\omega'_{IEH}}\right)\beta_{SA}$$

$$+ \left(\frac{\omega'_{IEV}}{\omega'_{IEH}}\right)(2\beta_{4TF} - \beta_{4TH}) - \frac{(2\omega'_{4\gamma F} - \omega'_{4\gamma H})}{\omega'_{IEH}}$$

Figure 7. Wheel-Speed-Modulation Azimuth Estimation Using Torque Output in Full-H Meru

Simulated Parameters:

$\alpha_{AZ} = 5 \times 10^{-6}$ Rad

$\alpha_{OA} = 100 \times 10^{-6}$ Rad

$\beta_{SA} = 50 \times 10^{-6}$ Rad

$\beta_T = \omega_Y = 0$

$(D_F)_T = 0.4$ Dyne-cm

$(D_0)_T = 0.02$ Dyne-cm

$(D_{00})_T = 0$

$(\ D_F)_T = 0.001$ Dyne-cm

Simulated Gyro Output:

Full Wheel Speed	M_{1F}	0.378400 Dyne-cm
	M_{2F}	0.384057 Dyne-cm
	M_{3F}	0.421331 Dyne-Cm
	M_{4F}	0.416212 Dyne-cm
Half Wheel Speed	M_{1H}	0.389200 Dyne-cm
	M_{2H}	0.392029 Dyne-cm
	M_{3H}	0.430666 Dyne-cm
	M_{4H}	0.428106 Dyne-cm

Figure 8. Simulated Data at Full and Half Wheel Speed

TRADITIONAL 4-POSITION GYROCOMPASSING ESTIMATES:

Parameter	Full-H	Half-H
α_{AZ} (μrad)	5.0	5.0
α_{OA} (μrad)	100.0	100.0
β_{SA} (μrad)	50.0	
$(\Delta D_F)_T$ (Dyne-cm)	0.001000	

WHEEL-SPEED-MODULATION AZIMUTH ESTIMATES IN μRAD:

Position	No Compensation	$(\Delta D_F)_T$ Compensation	α_{OA} Compensation	β_{SA} Compensation	$(\Delta D_F)_T$, α_{OA} Compensation	$(\Delta D_F)_T$, β_{SA} Compensation	α_{OA}, β_{SA} Compensation	$(\Delta D_F)_T$, α_{OA}, β_{SA} Compensation
OA↑/IAW	+133.6	+ 59.4	+ 33.6	+179.2	-40.6	+105.0	+79.2	5.0
OA↑/IAE	+ 76.3	+150.6	- 23.7	+ 30.7	+50.6	+105.0	-69.3	5.0
OA↓/IAW	+ 24.9	- 49.4	+124.9	- 20.7	+50.6	- 95.0	+79.3	5.0
OA↓/IAE	-214.8	-140.6	-114.8	-169.2	-40.6	- 95.0	-69.2	5.0

Figure 9. Comparison of Azimuth Estimates Using Simulated Data

Gyro PM-1 Output:

$\hat{M}_{1F}$ = 130.491 Full-H Meru

$\hat{M}_{2F}$ = 130.279 Full-H Meru

$\hat{M}_{3F}$ = 129.761 Full-H Meru

$\hat{M}_{4F}$ = 129.836 Full-H Meru

$\hat{M}_{1H}$ = 130.408 Full-H Meru

$\hat{M}_{2H}$ = 130.304 Full-H Meru

$\hat{M}_{3H}$ = 129.874 Full-H Meru

$\hat{M}_{4H}$ = 129.960 Full-H Meru

Traditional 4-Position Gyrocompassing Estimates:

Parameter	Full-H	Half-H
α_{AZ} (sec)	- 9.6	- 2.5
α_{OA} (sec)	-20.0	-26.5
β_{SA} (sec)	+ 45.2	
ΔD_F (Full-H Meru)	+0.045	

Wheel-Speed-Modulation Azimuth Estimates in Sec:

Position	No Compensation	ΔD_F, α^*_{OA}, β_{SA} Compensation
OA-Up, IA-West	-46.3	- 7.0
OA-Up, IA-East	-14.0	- 6.7
OA-Down, IA-West	+63.1	-26.5
OA-Down, IA-East	-69.2	-26.2

*Using average value from 4-position gyrocompassing estimates

Figure 10. Comparison of Azimuth Estimtes from PM-1 Data

Wheel-Speed-Modulation Azimuth Estimates in Sec:

Position	ΔD_F, $\bar{\alpha}_{OA}$, β_{SA} Compensation	ΔD_F, α_{OAF}, α_{OAH}, β_{SA} Compensation
OA-Up, IA-West	- 7.0	-16.8
OA-Up, IA-East	- 6.7	-16.5
OA-Down, IA-West	-26.5	-16.7
OA-Down, IA-East	-26.2	-16.5

Wheel-Speed-Modulation Azimuth estimation for hypothetical azimuth change between full and half wheel speed:

$$\hat{\alpha}_{AZ} = 2(\alpha_{AZ})_{FULL} - (\alpha_{AZ})_{HALF}$$

$\hat{\alpha}_{AZ}$ = - 16.7 SEC Using PM-1 4-position Gyrocompassing Estimates

Conclusion: Wheel-Speed-Modulation azimuth estimates are compatible with 4-position gyrocompassing estimates. However, the changes in azimuth and IA misalignment about OA with wheel speed are anomalous.

Figure 11. Compatibility of Wheel-Speed-Modulation and Traditional 4-position Gyrocompassing Analyses


DATE
FILME
8